



저작자표시-비영리-변경금지 2.0 대한민국

이용자는 아래의 조건을 따르는 경우에 한하여 자유롭게

- 이 저작물을 복제, 배포, 전송, 전시, 공연 및 방송할 수 있습니다.

다음과 같은 조건을 따라야 합니다:



저작자표시. 귀하는 원저작자를 표시하여야 합니다.



비영리. 귀하는 이 저작물을 영리 목적으로 이용할 수 없습니다.



변경금지. 귀하는 이 저작물을 개작, 변형 또는 가공할 수 없습니다.

- 귀하는, 이 저작물의 재이용이나 배포의 경우, 이 저작물에 적용된 이용허락조건을 명확하게 나타내어야 합니다.
- 저작권자로부터 별도의 허가를 받으면 이러한 조건들은 적용되지 않습니다.

저작권법에 따른 이용자의 권리는 위의 내용에 의하여 영향을 받지 않습니다.

이것은 [이용허락규약\(Legal Code\)](#)을 이해하기 쉽게 요약한 것입니다.

[Disclaimer](#)

2015년 8월
박사학위논문

메탄 수증기-이산화탄소 개질을 위한 메탈폼 촉매의 열-화학적 특성 연구

조선대학교 대학원

항공우주공학과

박 대 일

메탄 수증기-이산화탄소 개질을 위한 메탈폼 촉매의 열-화학적 특성 연구

Study on Thermal-Chemical Characteristics of Metallic
Foam Catalyst for Steam-CO₂ Reforming of Methane

2015 년 8 월 25 일

조 선 대 학 교 대 학 원

항 공 우 주 공 학 과

박 대 일

메탄 수증기-이산화탄소 개질을 위한 메탈폼 촉매의 열-화학적 특성 연구

지도교수 김 태 규

이 논문을 공학 박사학위신청 논문으로 제출함

2015 년 4 월

조 선 대 학 교 대 학 원

항 공 우 주 공 학 과

박 대 일

박대일의 박사학위논문을 인준함

위원장	조선대학교 조교수	<u>오 현 웅 (인)</u>
위 원	한국기계연 연구원	<u>이 대 훈 (인)</u>
위 원	한밭대학교 조교수	<u>이 종 광 (인)</u>
위 원	한국기계연 연구원	<u>조 성 권 (인)</u>
위 원	조선대학교 부교수	<u>김 태 규 (인)</u>

2015 년 6 월

조선대학교 대학원

Contents

Contents	i
LIST OF FIGURES	iv
LIST OF TABLES	vii
ABSTRACT	viii
Chapter 1. Introduction	1
Chapter 2. Research background	4
2.1. GTL technology	4
2.2. Reforming of Methane	6
2.3. Metallic foam	7
2.4. Perovskite-type structure	8
2.5. Polyol method	10
Chapter 3. Metallic foam catalyst	11
3.1. Preparation of catalyst	11
3.2. Characterization of the catalysts	15
3.2.1 X-ray diffraction (XRD)	15
3.2.2. Field emission scanning electron microscopy (FE-SEM)	15

3.3. Adhesion strength of the metallic foam catalyst	16
3.4. Heat transfer of the metallic foam catalyst	16
3.5. Steam-CO ₂ reforming of methane	19
3.6. γ -Al ₂ O ₃ /Ni foam characterization	23
3.7. Surface quality of the wash-coated catalyst	27
3.8. Adhesion strength of the wash-coated catalyst	31
3.9. Heat transfer characteristics of the wash-coated catalyst	33
3.10. Comparison of the Ni/ γ -Al ₂ O ₃ /Ni foam with the Ni/ γ -Al ₂ O ₃ pellet catalyst ...	36
3.11. Effect of temperature on the reactivity of the Ni/ γ -Al ₂ O ₃ /Ni foam catalyst ...	39
3.12. Effect of space velocity on the reactivity of the Ni/ γ -Al ₂ O ₃ /Ni foam catalyst ·	41
3.13. Catalytic activity of the wash-coated catalyst	43
3.14. Long-term durability of the Ni/ γ -Al ₂ O ₃ /Ni foam catalyst	46
Chapter 4. Perovskite-type catalysts (Polyol method)	50
4.1. Preparation of perovskite type catalyst	50
4.2. Characterization of perovskite type catalyst	52
4.2.1. H ₂ -temperature programmed reduction (H ₂ -TPR)	52
4.2.2. Fourier transform infrared spectrometry (FT-IR)	52
4.2.3. Thermogravimetric analysis (TGA)	52
4.3. XRD analysis	53
4.4. H ₂ -TPR profiles	56
4.5. FT-IR analysis	58
4.6. Reactivity of reforming	60
4.7. Carbon deposition (TGA)	62

4.8. Surface reaction mechanism	64
Chapter 5. Perovskite-type catalysts (Other sol-gel method)	69
5.1. Preparation of perovskite type catalyst	69
5.2. Characterization and Reaction test	70
5.3. Catalyst characterization	72
5.4. Effect of gelation agents on the reactivity of perovskite type catalyst	76
Chapter 6. Conclusion	78
Reference	80
Curriculum Vitae	

LIST OF FIGURES

Fig. 1. Schematic diagram for XTL technology	5
Fig. 2. Ni foam structure and SEM image of the Ni foam	7
Fig. 3. The schematic representation of the perovskite lattice structure	9
Fig. 4. Process of polyol method	10
Fig. 5. Ni/ γ -Al ₂ O ₃ /Ni foam catalyst: (a) bare Ni foam, (b) γ -Al ₂ O ₃ -supported Ni foam, and (c) Ni/ γ -Al ₂ O ₃ /Ni foam	13
Fig. 6. Experimental setup for the radial heat transfer measurements	18
Fig. 7. Flow diagram for modeling a SCR reactor by Aspen Plus	20
Fig. 8. Experimental setup for the steam-CO ₂ reforming of methane	22
Fig. 9. SEM images of the Ni/ γ -Al ₂ O ₃ /Ni foam: Bare Ni foam (a) $\times 30$, (b) $\times 6000$, and Ni/ γ -Al ₂ O ₃ /Ni foam (c) $\times 30$, and (d) $\times 6000$	24
Fig. 10. XRD patterns of the Ni/ γ -Al ₂ O ₃ /Ni foam at the different calcination temperature ..	25
Fig. 11. Weight fraction of the Al ₂ O ₃ wash-coat layer to a Ni foam as a function of the number of wash-coatings	28
Fig. 12. SEM images of the wash-coat layer at different Al ₂ O ₃ /AIP molar ratios: (a) bare Ni foam, (b) Al ₂ O ₃ /AIP=1, (c) Al ₂ O ₃ /AIP=3, (d) Al ₂ O ₃ /AIP=5, (e) Al ₂ O ₃ /AIP=7, and (f) Al ₂ O ₃ /AIP=9	30
Fig. 13. Nusselt numbers of the reactor packed with the γ -Al ₂ O ₃ pellets and wash-coated Ni foam	34
Fig. 14. Inlet and outlet temperatures as a function of the flow rate at the γ -Al ₂ O ₃ /Ni foam	

and γ -Al ₂ O ₃ pellets	35
Fig. 15. CH ₄ and CO ₂ conversions of the pellet and metallic foam catalyst as a function of temperature at a space velocity of 10,000h ⁻¹	37
Fig. 16. Temperature difference between the inlet and outlet of the pellet and Ni foam catalysts	38
Fig. 17. Syngas production rate and H ₂ /CO molar ratio of the pellet and metallic foam catalyst as a function of temperature at a space velocity of 10,000h ⁻¹	40
Fig. 18. CH ₄ conversion of the Ni/ γ -Al ₂ O ₃ /Ni foam catalyst as a function of the space velocity at 700 and 800°C	42
Fig. 19. CH ₄ and CO ₂ conversion of the bare Al ₂ O ₃ bead, bare Ni foam, Al ₂ O ₃ /Ni foam, and Ni/Al ₂ O ₃ /Ni foam	44
Fig. 20. (a) Syngas flow rate (H ₂ + CO) and (b) H ₂ /CO molar ratio of the bare Al ₂ O ₃ bead, bare Ni foam, Al ₂ O ₃ /Ni foam, and Ni/Al ₂ O ₃ /Ni foam	45
Fig. 21. Result of the durability test of the Ni/ γ -Al ₂ O ₃ /Ni foam catalyst at 800°C for 50 h at a space velocity of 130,000 h ⁻¹	48
Fig. 22. SEM images of the Ni/ γ -Al ₂ O ₃ /Ni foam catalyst after the durability test: (a) \times 30, (b) and (c) \times 250, and (d) \times 2000	49
Fig. 23. La _{0.8} Sr _{0.2} NiO ₃ / α -Al ₂ O ₃ catalyst	51
Fig. 24. XRD patterns of La _{0.8} Sr _{0.2} NiO ₃ perovskite-type catalysts at different PVP molarities: (P) perovskite, (S) SrCO ₃ , and (N) NiO	54
Fig. 25. TPR profiles of La _{0.8} Sr _{0.2} NiO ₃ perovskite-type catalysts at different PVP molarities	57
Fig. 26. FT-IR adsorption spectra of the perovskite-type catalysts at different PVP molarities	

.....	59
Fig. 27. Reactivity of the perovskite-type catalysts at different PVP molarities: (a) SCR of methane and (b) DR of methane, (■) CH ₄ conversion and (▲) CO ₂ conversion	61
Fig. 28. TGA analysis of perovskite-type catalysts and Ni catalyst after reacting for 12 h: (a) SCR of methane and (b) DR of methane	63
Fig. 29. Proposed surface mechanism over the reduced perovskite-type catalyst: (a) reaction of the carbon species with CO ₂ and (b) coke gasification with the addition of water	66
Fig. 30. XRD patterns of the perovskite-type catalysts after the reaction: : (●) SrCO ₃ , (▽) La ₂ O ₃ , (□) La ₂ O ₂ CO ₃ , and (◆) La ₂ NiO ₄	67
Fig. 31. SEM images of the perovskite-type catalysts: (a) before the reaction and (b) after the reaction	68
Fig. 32. Experimental setup for SCR and DR of methane reaction	71
Fig. 33. XRD patterns of the perovskite type catalysts according to the gelation agents; (a) PVA, (b) PAA and (c) EDTA agent	73
Fig. 34. FT-IR of the perovskite type catalysts according to the gelation agents; (a) EDTA, (b) PAA and (c) PVA agent	74
Fig. 35. H ₂ -TPR profiles of the perovskite-type catalyst according to the gelation agents; (a) PVA, (b) PAA and, (c) EDTA agent	75
Fig. 36. CH ₄ and CO ₂ conversions of the perovskite-type catalysts according to the gelation agents at different reactions; (a) DR of methane and (b) SCR of methane	77

LIST OF TABLES

Table 1.	Preparation conditions of Ni/ γ - Al_2O_3 /Ni foam and Ni/ γ - Al_2O_3 pellet catalysts	· 14
Table 2.	Simulation results estimated by ASPEN plus in the SCR of methane	····· 21
Table 3.	Particle size of the Ni/ γ - Al_2O_3 /Ni foam catalyst after the calcination	····· 26
Table 4.	Number of wash-coating repetitions to obtain ~20 wt.% of wash-coat according to the Al_2O_3 /AIP molar ratio	····· 29
Table 5.	Fall-off rate of the wash-coated Ni foams with different Al_2O_3 /AIP molar ratios	·· ··· ····· 32
Table 6.	SrCO_3 particle sizes at different PVP molarities	····· 55

ABSTRACT

Study on Thermal-Chemical Characteristics of Metallic Foam Catalyst for Steam-CO₂ Reforming of Methane

by Park, Daeil

Advisor : Prof. Kim, Taegy, Ph. D.

Department of Aerospace Engineering,

Graduate School of Chosun University

GTL 기술은 2000년대 들어 석유 자원의 한계성, 원유 가격의 상승 및 환경 오염문제로 인해 각광 받고 있는 기술이다. GTL 기술은 천연가스의 주성분인 메탄을 Ni계 촉매를 사용하여 개질반응 시켜 수소와 일산화탄소로 이루어진 합성가스를 제조하고, 얻어진 합성가스를 FT합성을 통하여 고 비점의 탄화수소를 얻게 된다. 마지막으로 업그레이드 공정을 통해 얻어진 액체 연료는 유황 및 방향족 화합물의 함유량이 적어 청정 연료로 간주 된다. 최근 개발이 힘든 중소규모의 한계가스전이나 수반가스전을 GTL 기술을 적용시킨 GTL-FPSO를 통하여 개발이 가능하다는 점에서 많은 관심을 받고 있다. GTL-FPSO 공정의 경우 해상에서 진행되는 공정임을 고려해서 해상환경조건(파도, 조력, 바람, 해수 온도 등)등의 가혹한 조건을 견딜 수 있는 촉매 개발이 필요하다. 기존에 연구되던 펠렛 기반의 촉매의 경우 구조적 강도나 열전도성이 떨어져 해상환경에 적용시키기에는 제약조건이 많다. 펠렛 기반 촉매의 단점을 보완하기 위해 기계 및 구조적 강도가 우수하고 열전달 특성이 우수한 금속폼 지지체를 사용하여 촉매를 제조하는 방법이 관심을 받고 있다. 금속폼 지지체를 반응에 사용하기 위해서는 졸겔법이나 슬러리법으로 제조된 담체를 워시코팅 후 촉매를 함침 시켜 사용하는데 두 가지 방법에는 각각의 장·단점이 존재한다.

본 연구에서는 졸겔법과 슬러리법의 장점만을 혼합하여 졸겔-슬러리 하이브리드

코팅법을 사용하여 위시코팅 메탈폼 지지체를 제조하였다. 하이브리드 코팅법의 장점은 균일한 코팅 표면을 얻을 수 있고, 담체 로딩량을 조절할 수 있는 점이다. 두 가지 방법을 혼합하였기 때문에 졸겔과 슬러리 코팅법의 최적의 포인트를 찾아야 한다. 본 연구에서는 첨가물의 비율을 조절하여 최적의 코팅 조건을 찾고, 실험 및 분석을 통하여 검증하였다.

첫 번째로 Al_2O_3 와 AIP를 1~9까지 5가지 샘플을 제조하여 Al_2O_3 /AIP 몰 비율에 따른 메탈폼 표면 상태를 SEM사진을 통해 확인할 수 있었다. Al_2O_3 가 코팅된 메탈폼 지지체의 SEM 사진을 보면 Al_2O_3 /AIP 몰 비율이 5일 때 균일한 메탈폼 표면을 확인할 수 있었는데, 5 이외의 다른 샘플의 경우 표면에 균열이 심각하게 발생돼 반응에 사용하였을 때 부정적인 영향이 나타날 것이라 판단된다. 추가로 Fall-off rate 실험을 수행하여 메탈폼 지지체와 담체의 접착 강도를 확인하기 위해 10시간과 50시간에 걸쳐 ultrasonic에 넣고 실험을 수행하였다. 실험 결과 Al_2O_3 /AIP 몰 비율이 5일 때 떨어지는 담체량이 가장 적었으며, 위 결과들을 바탕으로 Al_2O_3 /AIP 몰 비율이 5일 때 최적의 위시코팅 조건이라고 판단된다.

두 번째로 최적의 조건으로 제조된 Al_2O_3 /Ni foam과 기존에 많이 사용되는 Al_2O_3 펠렛 지지체와의 열전달 성능 및 반응성의 차이를 실험을 통하여 확인하였다. 우선 열전달 성능 비교를 위해 반응기에 위시코팅된 메탈폼과 펠렛 지지체를 넣고 비활성 가스인 N_2 를 100~500cc까지 흘려 두 지지체간의 입·출구의 온도 차이를 측정하여 Nu 수를 계산하였다. 계산 결과 위시코팅된 메탈폼이 펠렛 지지체에 비해 높은 Nu수를 보였으며, N_2 유량이 증가 할수록 두 샘플간의 Nu 수 차이가 커지는 것을 확인하였다. 위 결과를 바탕으로 위시코팅된 Al_2O_3 /Ni foam이 펠렛 촉매에 비해 높은 열전도율을 보이는 것을 확인 하였다. 높은 열전도율이 반응에 미치는 영향을 알아보기 위해 두 지지체에 Ni 촉매를 함침 시켜 제조 후 수증기-이산화탄소 복합개질 반응을 통해 반응성을 확인하였다. 실험 결과 모든 온도 구간에서 Ni/ Al_2O_3 /Ni foam 촉매가 Ni/pellet 촉매 보다 CH_4 및 CO_2 전환율이 높게 나타났다. 위 결과를 바탕으로 열 전달 성능이 반응에 크게 영향을 미치는 것을 확인 하였으며, 특히 저온 반응으로 갈수록 메탈폼의 효과가 극대화 된다고 판단된다.

Ni계 촉매를 반응에 사용할 경우 많은 양의 탄소 침적이 발생되는데, 기존 Ni 촉매와 동일한 성능을 가지면서 탄소 침적이 적게 발생하는 페롭스카이트 촉매를 추가로 연구하였다. 대부분의 페롭스카이트 촉매가 분말형태로 사용하기 때문에 상용공정에는

적용이 힘들다. 이를 극복하기 위해 페롭스카이트 촉매를 메탈폼에 코팅시키는 연구를 수행하였다. 기존의 페롭스카이트 제조법의 경우 메탈폼에 코팅하였을 때 부풀어 오르거나 폭발이 발생해 코팅에 적합하지 못하기 때문에 본 논문에서는 폴리올법을 페롭스카이트에 응용하여 촉매를 제조하였다. 제조된 촉매는 다양한 분석과 실험을 통하여 검증하였으며, 폴리올법에 사용되는 PVP 물질의 농도를 조절하여 최적의 조건을 찾아내었다. 실험 및 분석결과 PVP 몰수가 1일 때 수증기-이산화탄소 개질 및 건조 개질 반응에서 CH_4 과 CO_2 전환율이 가장 높았으며, XRD 및 TPR 분석을 통해서도 1M이 최적의 조건임을 확인 하였다. 마지막으로 Ni촉매와 페롭스카이트 촉매의 탄소 침적량을 TGA로 비교하였고, 페롭스카이트 촉매가 우수한 탄소 침적 저항성을 보인 것을 확인하였다.

실험 결과를 바탕으로 합성가스 생산량이 $0.08\text{Nm}^3/\text{hr}$ 급인 Ni foam 기반 반응기를 제작 할 경우 펠렛 지지체 기반 반응기에 비해 약 38.1%의 부피감소 효과를 볼 수 있었다. 본 연구를 통하여 메탈폼 지지체를 사용함으로써 반응성뿐만 아니라 반응기의 부피 감소에도 기존 지지체 촉매에 비해 우수함을 증명하였다.

Chapter 1. Introduction

Gas to liquids (GTL) technology has been mainly developed to produce clean synthetic fuels and to transform gas into liquid for more convenient transportation. Natural gas, which is exhaust from an oil field and is not applicable economically due to the limited reserves, can be converted to synthetic liquid fuels using the GTL process [1]. GTL technology is being developed as a new business model by major oil companies because of its merits in terms of the exploitation of small-scale undeveloped gas resources and the alternative to oil depletion.

The GTL process consists of three parts; reforming process, Fischer-Tropsch (FT) synthesis and upgrading process. The reforming process involves the conversion of methane (CH_4) to a syngas composed of hydrogen (H_2) and carbon monoxide (CO). The FT reaction is a synthesis reaction to obtain a high hydrocarbon containing wax as the main species. Finally, a clean synthesis fuel, such as a diesel, kerosene, jet fuel, gasoline and naphtha, can be produced through an upgrading process. Recently, there has been increasing interest in clean synthetic fuel production from stranded and associated gas fields on ships using GTL-FPSO (floating production, storage and offloading) process [2].

Steam- CO_2 reforming (SCR) is a combination of steam reforming and dry reforming. The H_2/CO molar ratio of syngas for FT synthesis can be controlled by adjusting the steam/ CO_2 molar ratio [3]. Water and CO_2 can be obtained easily from a submarine gas fields. The water can be obtained by desalination process of the seawater and the CO_2 of 15-80% is included in the submarine gas fields [4]. Therefore, SCR is the most suitable reforming process for GTL-FPSO. The SCR of methane reaction consists of three main reactions; Steam reforming, water-gas shift reaction and dry reaction. Additional reactions are involved including CO_2 methanation, CO methanation, methane decomposition, boudourd reaction and coke gasification.

In general, the reforming reaction employs noble metals, such as Pt, Pd and Rh and non-noble metals, such as Co, Ni and Fe [5-8]. The catalytic activity is strongly dependent on the reaction temperature, which is an important factor determining the reformer performance. On the other hand, the widely used pellet supports show low thermal

dispersion because of its low thermal conductivity. Therefore, cold or hot spots are formed on the catalyst surface during reforming, particularly as the reformer scale is increased. Hot spots can damage the catalyst and cold spots can decrease the catalytic activity. Therefore, a uniform temperature distribution through the SCR reaction is very important for the SCR reactor design [9].

Recently, metallic foam catalysts with high thermal conductivity, uniform thermal dispersion and high mechanical strength have been studied widely. The metallic foam is defined as a porous metal inside which many pores are formed. As a catalyst support, the metallic foam can improve the catalytic activity because of its high specific surface area. In addition, the metallic foam can improve heat and mass transfer, and can minimize the pressure drop because of its porous structure [10]. In particular, the metallic foam can remove the hot and cold spots on the catalysts in exothermic and endothermic reactions [11].

The metallic foam does not have high reactivity itself as a catalyst. Therefore, a porous catalyst should be coated on the surface of the metallic foam. The catalyst is difficult to coat directly on the metallic foam. As an alternative, the surface of metallic foam is pretreated by a wash-coating with a high porous material. Two methods are used widely for wash-coatings; sol-gel method and slurry method. The sol-gel method uses coating materials with organic agents, which are dissolved in distilled water. The pH of the aqueous solution is controlled by adding an acid. A sol is obtained after drying for a few hours at room temperature [12]. On the other hand, the slurry method uses a coating material with binder agents, which are dissolved in distilled water. A slurry in a liquid phase is obtained [13]. In both methods, the metallic foam can be wash-coated using either a sol or slurry. Using the sol-gel method, a uniform wash-coated layer on the surface of metallic foam can be obtained. On the other hand, the loading for one coating is so low that the wash-coating should be repeated to obtain a sufficient catalyst loading. In contrast, the slurry method can provide a high loading in a single coating but the wash-coated layer is not uniform and the metallic foam is coated layer by layer. In addition, the pores can be clogged with an accumulated lump and cracks can occur easily on the non-uniform and thick wash-coated layer.

In this study, the SCR of methane reaction over support catalyst has been investigated

in a fixed bed reactor system for GTL-FPSO process. The metallic support catalyst were prepared by hybrid technique of sol-gel and slurry methods was used to obtain the optimal conditions for wash-coating the metallic foam. And the metallic foam catalyst was compared with the existing Al_2O_3 -pellet catalyst. Also, a perovskite-type catalyst was prepared by polyol method, and it was characterized by various analytical techniques.

Chapter 2. Research background.

2.1. GTL technology

The speculation of high oil prices has driven great attention toward synthetic oil produced from natural gas or coal. The present technologies for synthetic oil production include GTL coal-to-liquid (CTL), biomass-to-liquid (BTL) [14]. Generally, CTL has received most of the attention to date, but there is increasing investment and technological development in GTL because of dramatic declines in the price of natural gas due to the rapid increase of its production [15].

The XTL process consists of three processes; reforming, FT synthesis and upgrading process, as shown in Fig. 1. The reforming process involves the conversion of methane from natural gas to syngas, which is composed of H_2 and CO. FT synthesis is a reaction to obtain high boiling point hydrocarbons as the main species. Subsequently, a clean synthetic fuel can be produced through an upgrading process, such as diesel, kerosene, gasoline and naphtha. In general, reforming is needed to produce syngas with a H_2/CO molar ratio that is suitable to the FT synthesis reaction over Fe or Co based catalyst. Co-based catalysts show the optimum activity from a H_2/CO molar ratio of 2 [16].

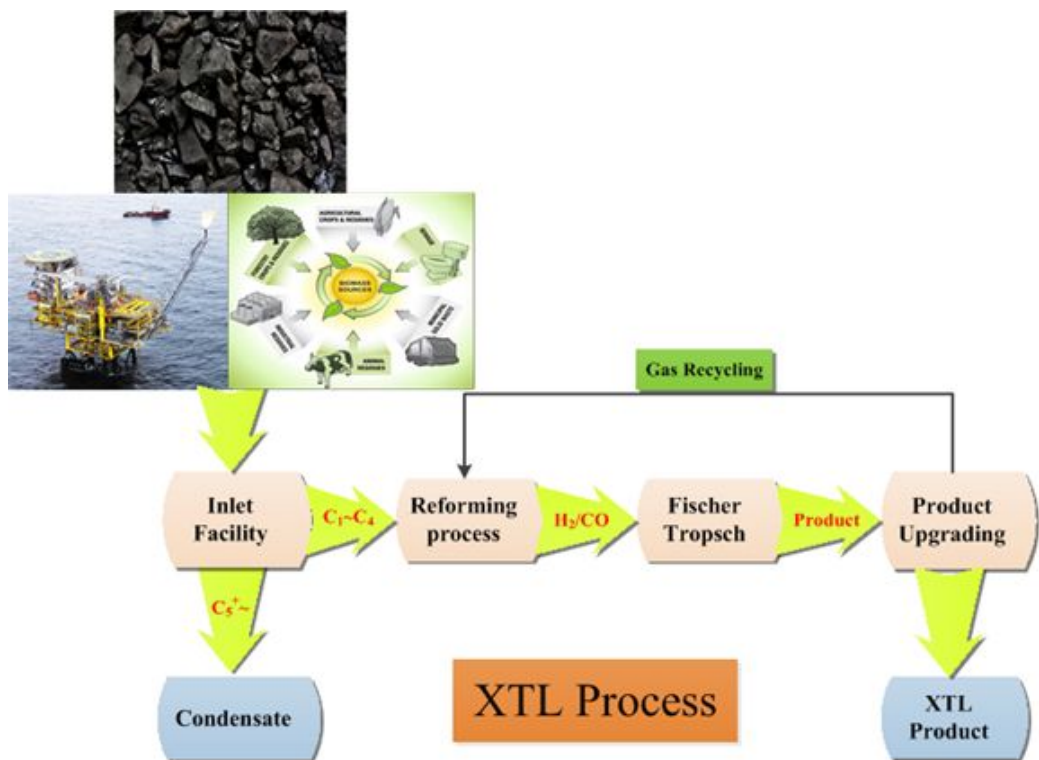
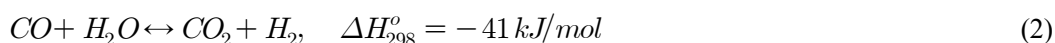
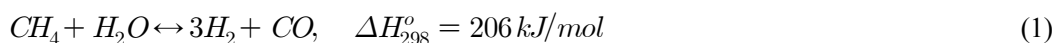


Fig. 1. Schematic diagram for XTL technology

2.2. Reforming of Methane

A reforming process is needed to produce the syngas from natural gas. the reforming process includes steam reforming, dry reforming, partial oxidation and auto-thermal reforming. Steam reforming involves the conversion of CH₄ with H₂O, which is abundant in the ocean, and might be suitable to GTL-FPSO applications. On the other hand, the steam reforming produces syngas with a H₂/CO molar ratio of 3-4. Therefore, an additional process to adjust the H₂/CO molar ratio is needed because the FT synthesis requires a H₂/CO molar ratio of 2 [17-18]. Dry reforming utilizes CO₂, which is a typical greenhouse gas, and might be suitable for GTL-FPSO applications because the natural gas in gas fields contains a large quantity of CO₂. On the other hand, the reformat gas contains a high CO content. Therefore, dry reforming does not meet the H₂/CO molar ratio for FT synthesis [19-20]. Partial oxidation is unsuitable for GTL-FPSO applications because it is difficult to control the hot spots and explosion danger caused by the high reforming temperature, even if it meets the H₂/CO molar ratio for FT synthesis [21-22]. Auto-thermal reforming, which is a combination of steam reforming and partial oxidation, can solve the drawbacks of partial oxidation. On the other hand, it requires an air separate unit (ASU), which is too bulky to equip it on a ship taking a severe space restriction [23-24].



The CH₄ steam reforming produces H₂ and CO, as expressed in Eq. (1). CO with H₂O is converted to H₂ by a WGS reaction, as expressed in Eq. (2). CO₂ is reacted with CH₄, as expressed in Eq. (3), to synthesis gas.

Noble, metals, such as Pt, Pd and Ru are mostly used as catalysts for reforming but

these metals are very expensive. Recently, it was reported that non-noble metals, such as CO and Ni, also have high reactivity on the reforming reaction.

2.3. Metallic foam

Metallic foam catalysts with high thermal conductivity, uniform thermal dispersion and high mechanical strength have been studied widely. The metallic foam is defined as a porous metal inside which many pores are formed, as shown in Fig. 2. The metallic foam is classified into two types; open cell and closed cell [25-26]. The closed cell-type metallic foam has pores that not are interconnected, whereas the pores are interconnected in the open cell type metallic foam. Therefore, a fluid can pass easily through the metallic foam. Consequently, the open cell-type metallic foam has been used widely in a range of industrial fields [27]. The cell size is indicated as pores per inch (PPI). Mostly, 5-100 PPI foams have been used, of which the porosity is approximately 80-97% [28]. As a catalyst support, the metallic foam can improve the catalytic activity because of its high specific surface area. In addition, the metallic foam can improve heat and mass transfer, and can minimize the pressure drop because of its porous structure [29]. In particular, the metallic foam can remove the hot and cold spots on the catalysts in exothermic and endothermic reactions [30].

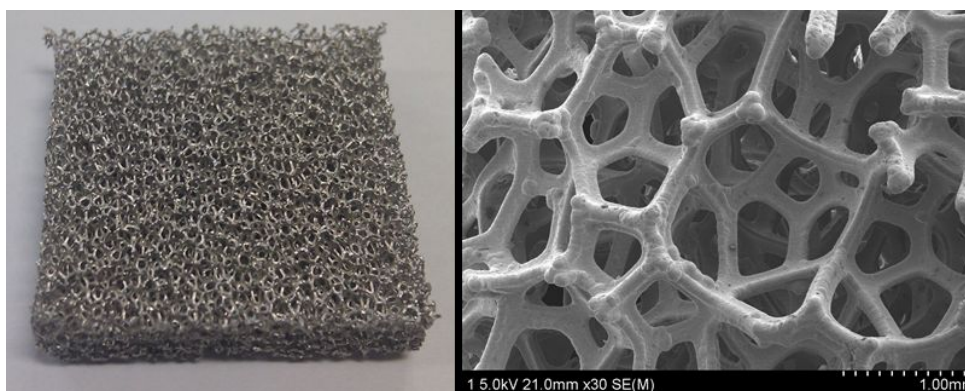


Fig. 2. Ni foam structure and SEM image of the Ni foam.

2.4. Perovskite-type structure

Perovskite-type catalysts can be used for the reforming reaction to improve the thermal stability. Perovskite-type structure have an ABO_3 structure, as shown in Fig. 3. The A site is occupied by a rare-earth or alkali-earth metal, such as La, Sr or Br, which determines the thermal stability of the catalyst. The B site is occupied by a 3d transition metal, such as Ni, Co or Fe, which determines the catalytic activity [31-34]. Additionally, their combination can also occupy the A and B sites. The more general, comprehensive structure of a perovskite-type catalyst is $A_{1-x}A'_xB_{1-y}B'_yO_3$, where x and y represent the degrees of substitution. The 3d transition metal, B or B', stabilizes the oxidized state. Furthermore, perovskite has a high mobility of oxygen ions and a high structural stability [35-38]. For these reason, perovskite-type catalysts have been widely used in reforming processes at high temperature.

There are several methods for producing perovskite-type catalysts, such as the sol-gel Pechini method and other sol-gel methods [39-42]. Although the Pechini method has been widely used because of its simplicity in preparation, the prepared catalyst lacks reproducibility due to factors involved during hydrolysis and condensation. Therefore, perovskite-type catalysts have recently been prepared by other sol-gel methods. Generally, a gelation agent like polyacrylic acid (PAA) or polyvinyl alcohols (PVA) is needed during the sol-gel process.

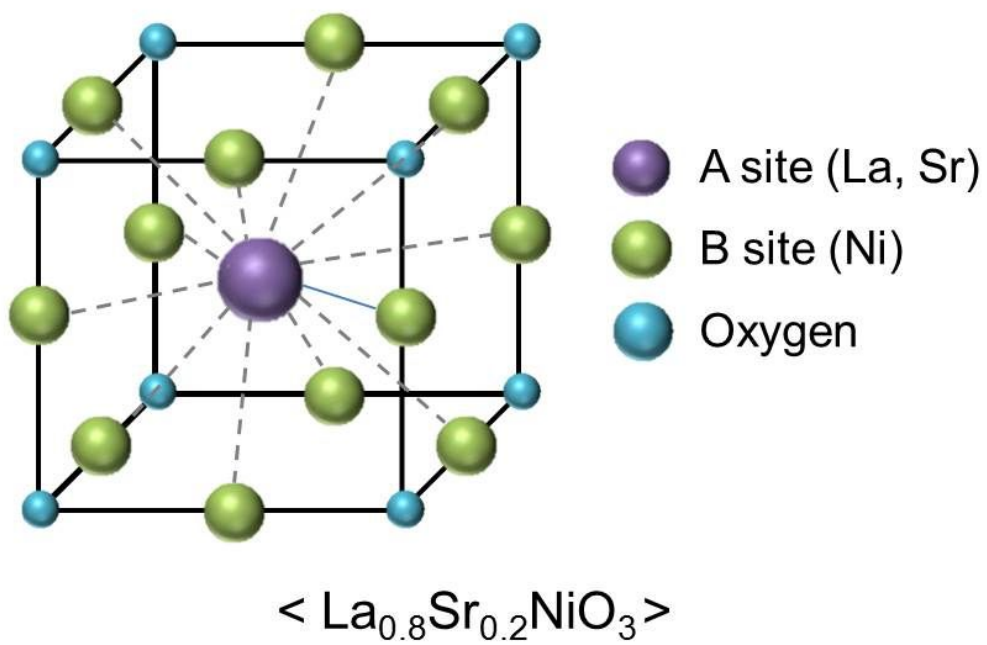


Fig. 3. The schematic representation of the perovskite lattice structure.

2.5. Polyol method

The polyol method is a well-known alcohol reduction method and can be considered a solvothermal method [43-44]. It has been used for the synthesis of monodisperse non-agglomerated metals, such as Co, Ni, Cu and noble metals that form micron and submicron-scale particles. Generally, a liquid polyol like ethylene glycol (EG), 1,2-propandiol, triethylene glycol or diethylene glycol is used as the solvent and mild reducing agent in the polyol method, as shown in Fig. 4. The metal ions decrease in size through reduction-oxidation reaction between the metal precursor and solvent. For this process, the metal precursor is suspended or dissolved by a liquid polyol.

These suspensions are heated to form metal particles. The addition of a polymer stabilizer such as polyvinyl-pyrrolidone (PVP) can prevent the metal particles from agglomerating during the heat treatment, resulting in uniformly sized metal nanoparticles. The addition of the multifunctional PVP ligand results in nanoscale particles that form nanocrystals; microscale particles are obtained when the stabilizer is excluded. Therefore, the polyol method makes it simple and easy to prepare the catalyst. In addition, the size and shape of the nanoparticles can be controlled by adjusting the PVP concentration [45].



Fig. 4. Process of polyol method

Chapter 3. Metallic foam catalyst

3.1. Preparation of catalyst

The metallic foam catalyst is composed of Ni as an active site for the SCR reaction, γ - Al_2O_3 layer as a support of the Ni sites, and the Ni foam as a substrate for the γ - Al_2O_3 support, as shown fig. 5. Nickel nitrate[$\text{Ni}(\text{NO}_3)_2 \cdot 6\text{H}_2\text{O}$, SAMCHUN PURE CHEMICAL Co.]] was used as a precursor of the Ni catalyst. The Ni foam (Pore Tech Co.) was selected as a substrate of the catalyst. Ni foam has a network structure with a porosity and density of 40 ppi(pore per inch) and 0.339g/cm^3 , respectively. The thermal conductivity of the Ni foam was $\sim 90\text{W/m-K}$, which is 3.6 times higher than that of Al_2O_3 ($\sim 25\text{ W/m-K}$)

The catalyst could not be coated directly on the surface of the metallic foam. A thin layer of γ - Al_2O_3 as the catalyst support was wash-coated on the Ni foam using a sol-gel method. After wash-coating, the precursor of the Ni catalyst was impregnated on the γ - Al_2O_3 support. Consequently, the Ni/ γ - Al_2O_3 /Ni foam catalyst was obtained. The detailed procedure for catalyst preparation is as follow.

Aluminum isopropoxide (Alfa Aesar Co.) was dissolved in distilled water, and then polyvinyl alcohol (Alfa Aesar Co.) as a binding agent was added to the aqueous solution. The pH of the aqueous solution was controlled by adding HNO_3 (JUNSEI) and the pH was maintained at 2.0. After drying for 2 h at room temperature, a transparent sol was prepared. $3\mu\text{m}$ Al_2O_3 (Alfa Aesar Co.) was added to the prepared sol in order to increase its viscosity and Al_2O_3 content in the sol. After stirring for 1 h, the Al_2O_3 sol for wash-coating was prepared.

The Ni foam was cut to the desired size and shape. as shown in Fig. 5 (a). A piece of Ni foam was immersed into a 10% HCl solution (SK Chemicals Co.) to remove contaminants from the Ni foam surface. After rinsing in distilled water, the Ni foam dried at a convection oven at 120°C for 1 h. The Al_2O_3 sol was wash-coated on the prepared Ni foam using a dip-coating method. The wash-coating process was repeated to obtain the desired weight fraction. The wash-coated Ni foam was dried at 100°C for 12 h and pre-calcined at 300°C in air. Fig. 5 (b) shows the prepared γ - Al_2O_3 /Ni

foam. The weight fraction of the Al_2O_3 layer to the Ni foam was 19.59 wt.%.

Finally, the Ni catalyst was coated on the prepared $\gamma\text{-Al}_2\text{O}_3/\text{Ni}$ foam using a wet-impregnation method. The precursor solution was prepared by dissolving $\text{Ni}(\text{NO}_3)_2$ in distilled water. The $\gamma\text{-Al}_2\text{O}_3/\text{Ni}$ foam was immersed into the precursor solution for 4 h. The bath temperature was maintained at 50°C during impregnation. After impregnation, the sample was dried at 100°C for 12 h and calcined in air at 800°C for 5 h. The weight fraction of the Ni catalyst to the $\gamma\text{-Al}_2\text{O}_3$ supported on Ni foam was 19.96 wt.%. The weight fraction of the Ni catalyst to the total weight including $\gamma\text{-Al}_2\text{O}_3$ and Ni foam was 4.0%. Fig. 5 (c) shows the prepared $\text{Ni}/\gamma\text{-Al}_2\text{O}_3/\text{Ni}$ foam catalyst.

For comparison with the metallic foam catalyst, the Ni catalyst supported on $\gamma\text{-Al}_2\text{O}_3$ pellet (Alfa Aesar Co.) was prepared using a wet impregnation method. The weight fraction of the Ni in the pellet catalyst was the same as that in the metallic foam catalyst to compare the reactivity of the SCR reaction between both catalysts. Table 1 lists the preparation conditions for both catalysts.

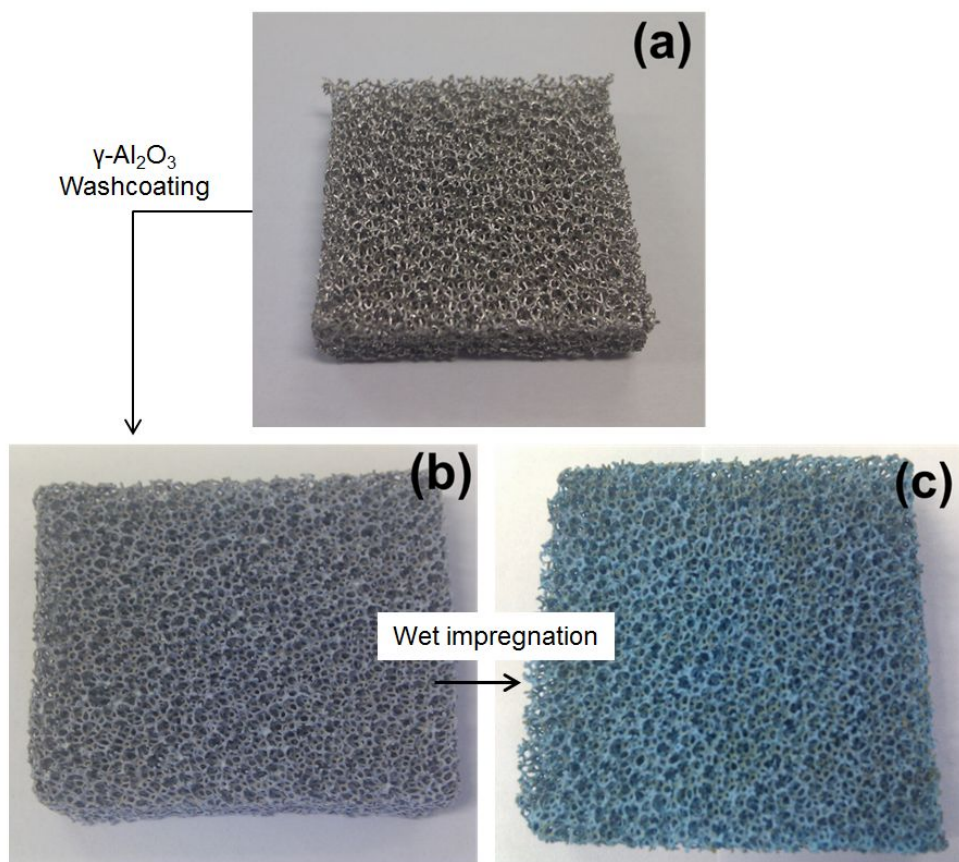


Fig. 5. Ni/γ-Al₂O₃/Ni foam catalyst: (a) bare Ni foam, (b) γ-Al₂O₃-supported Ni foam, and (c) Ni/γ-Al₂O₃/Ni foam.

Table 1 Preparation conditions of Ni/ γ -Al₂O₃/Ni foam and Ni/ γ -Al₂O₃ pellet catalysts.

Catalyst	Ni wt.% / γ -Al ₂ O ₃	γ -Al ₂ O ₃ wt.% /Ni foam	Catalyst wt.% [*]	Impregnation temperature (°C)	Calcination temperature (°C)
Ni/ γ -Al ₂ O ₃ Ni foam	19.96	19.59	4.0	50	800
Ni/ γ -Al ₂ O ₃ pellet	20.50	-	-	50	800

*Weight fraction of Ni catalyst to the total weight.

3.2. Characterization of the catalysts

The catalysts before and after the reaction were characterized by different analytical techniques, such as X-ray diffraction (XRD), field emission scanning electron microscopy (FESEM).

3.2.1. X-ray diffraction (XRD)

Metallic foam catalyst were characterized by X-ray diffraction (XRD) using a Rigaku D/MAX-3C diffractometer with $\text{CuK}\alpha_1 = 1.5406\text{\AA}$ and $\text{CuK}\alpha_2 = 1.5444\text{\AA}$. The diffractometer was operated at 40kV and 30mA. The diffraction patterns were scanned for 2θ values in the range of $20\text{--}80^\circ$ with a scan-step size of 0.03° and scan-step time of 1 s. The particle sizes was calculated using the Scherrer equation shown in Eq. (4)

$$\tau = \frac{K\lambda}{\beta \cos \theta} \quad (4)$$

where τ is the mean size of the ordered (crystalline) domains, which may be smaller or equal to the grain size. K is the dimensionless shape factor, which typically has a value of 0.9. The λ and β factors are the X-ray wave length and line broadening at half the maximum intensity (FWHM), respectively.

3.2.2. Field emission scanning electron microscopy (FE-SEM)

The surface morphology of the catalyst before and after the reaction was analyzed by field emission scanning electron microscopy (FESEM, Hitachi S-4800)

3.3. Adhesion strength of the metallic foam catalyst

The coating quality of the catalyst layers that had been coated using the wash-coating solution at different $\text{Al}_2\text{O}_3/\text{AIP}$ molar ratios was evaluated. The adhesion strength of the wash-coat layers with the Ni foam was evaluated by measuring the fall-off rate [46]. Ultrasonic bath (HWASHIN Powersonic 510) was used to provide physical damage to the wash-coated Ni foam. The frequency and nominal power of the ultrasonic were 45kHz and 500W, respectively. The fall-off rate was defined as the weight loss after the fall-off test. Five samples of the wash-coated Ni foam prepared at different $\text{Al}_2\text{O}_3/\text{AIP}$ ratios were tested and their weights were measured 10 and 50 h after initiating the fall-off test using a high resolution balance (AND GF-600).

3.4. Heat transfer of the metallic foam catalyst

The Nusselt number was used to evaluate the improvement in heat exchange between the wash-coated Ni foam and gaseous reactants. The Nusselt number is defined as Eq. (5) [47].

$$N = \frac{h_e D}{k_c} \quad (5)$$

where h_e , k_c and D are a convective heat transfer coefficient, thermal conductivity of the reactants and characteristic length, respectively. Fig. 6 shows the experimental setup for measuring the temperatures of the reactor to obtain the Nusselt number of radial heat transfer. A 1 inch diameter tubular reactor made of the stainless steel (SUS316) was used, and thermocouples were located at the inlet (T_i), middle (T_m), outlet (T_o) and wall (T_w). The wash-coated Ni foam was packed into the reactor. The wash-coated Ni foam was packed into the reactor.

The $\gamma\text{-Al}_2\text{O}_3$ pellets with the same volume were also packed for comparison. N_2 was used as a feed gas and the flow rate was controlled to 100–500 mL/min using a mass flow controller (MFC, NFS TSC-210). The wall temperature was fixed to 200°C in the

present study.

In the configuration of the reactor packed with the wash-coated Ni foam, he was obtained by measuring the wall temperature (T_w) and the centerline temperatures of the reactor inlet (T_i) and outlet (T_o). The heat is transferred from the wall to the center in the tubular reactor. The Nusselt number for the radial heat transfer was calculated by integrating the local heat transfer rate across the whole bed of the reactor as Eq. (6).

$$Nu = \frac{\rho C_p r_o^2 u}{k_c L} \ln \frac{T_w - T_i}{T_w - T_o} \quad (6)$$

where ρ and C_p are a density and specific heat of the fluid in the reactor respectively. r_o , L and u are the radius, length of the reactor and the flow rate, respectively. T_w , T_i and T_o are temperatures located at the wall, inlet and outlet, respectively [48-49].

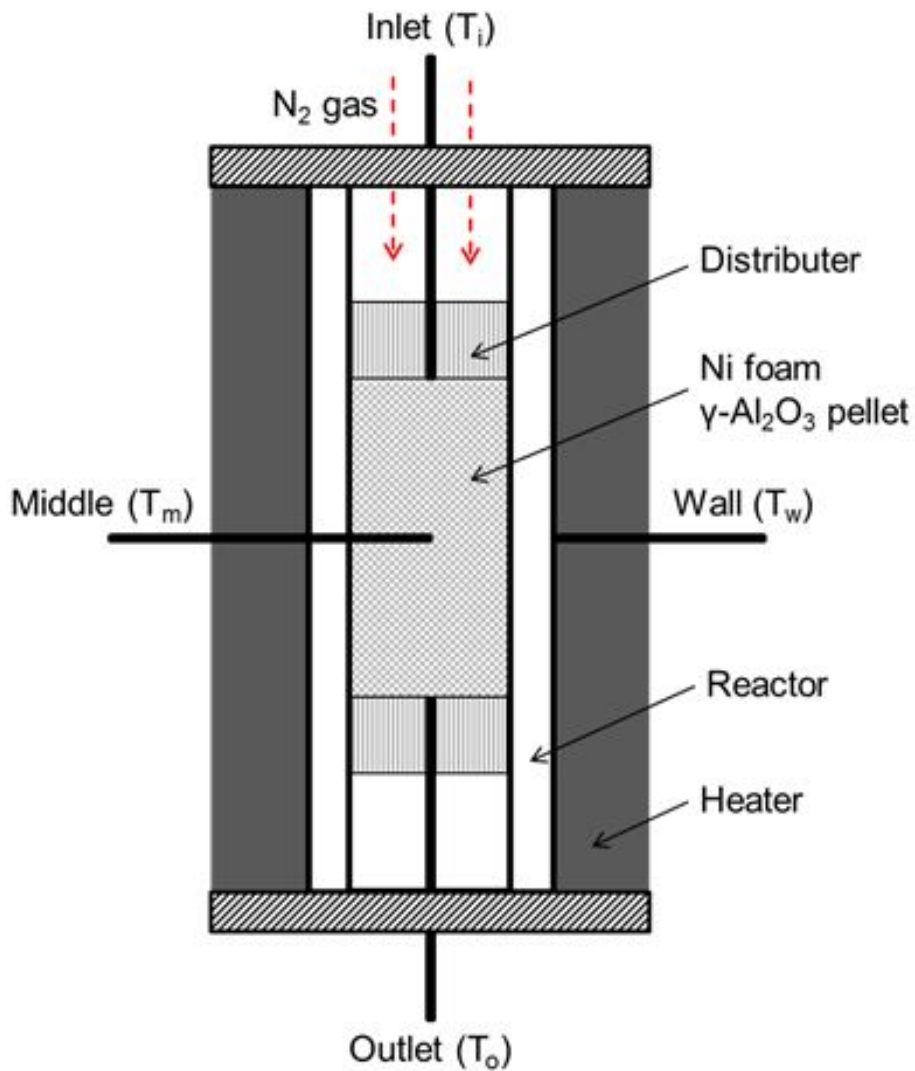


Fig. 6. Experimental setup for the radial heat transfer measurements.

3.5. Steam-CO₂ reforming of methane

Before examining the reactivity of the catalysts, the optimal feed composition for the SCR reaction was determined by using ASPEN Plus simulation. A Gibbs reactor was used to simulate the SCR reaction, and a heater and mixer were provided in the molar ratio of the feed gases (CH₄:H₂O:CO₂) to obtain a H₂/CO molar ratio optimized to the FT reaction. Fig. 7 and Table 2 presents the H₂O and CO₂ compositions were varied in the range of 0.8-1.1 and 1.7-2.1 at a fixed CH₄ composition (1.0 mol), respectively. The reaction temperature was fixed to 800°C.

Fig. 8 presents the experimental apparatus for the steam-CO₂ reforming of methane on the Ni-Al₂O₃/Ni foam catalyst. A SUS316 tube, 1.27cm in diameter and 40 cm in length, was used for the reaction. The prepared Ni-Al₂O₃/Ni foam catalyst was packed in the reactor and the catalyst weight was 0.5g. The reaction temperature ranged from 450 to 950°C, and the gas hourly space velocity (GHSV) was varied from 10,000 to 40,000h⁻¹. The Ni/γ-Al₂O₃ pellet catalysts were diluted with inert Al₂O₃ pellets in order to regulate the space velocity. Thus, both catalysts were evaluated under the same reaction conditions. All experiments were performed at atmospheric pressure. The long-term durability of the catalyst was examined at a reaction temperature of 850°C and a GHSV of 130,000h⁻¹. All catalysts were reduced at 800 °C for 2 h in a H₂ atmosphere with a flow rate of 50 mL/min. The CH₄ and CO₂ were supplied by a MFC and H₂O was supplied by a liquid piston pump. The CH₄ and CO₂ were mixed with H₂O after vaporizing at 300°C. The space velocity was fixed to 10,000 h⁻¹. The dry product gases after separating the liquids in the products through a liquid trap were analyzed by GC (gas chromatography) equipped with a thermal conductivity detector (TCD) and a flame ionized detector (FID). The GC was calibrated with a standard gas to determine the concentration of CH₄, CO₂, CO, H₂ and N₂. The CH₄ and CO₂ conversions were calculated from the product composition under each reaction condition. The carbon balance was correct within 10% at all experiments.

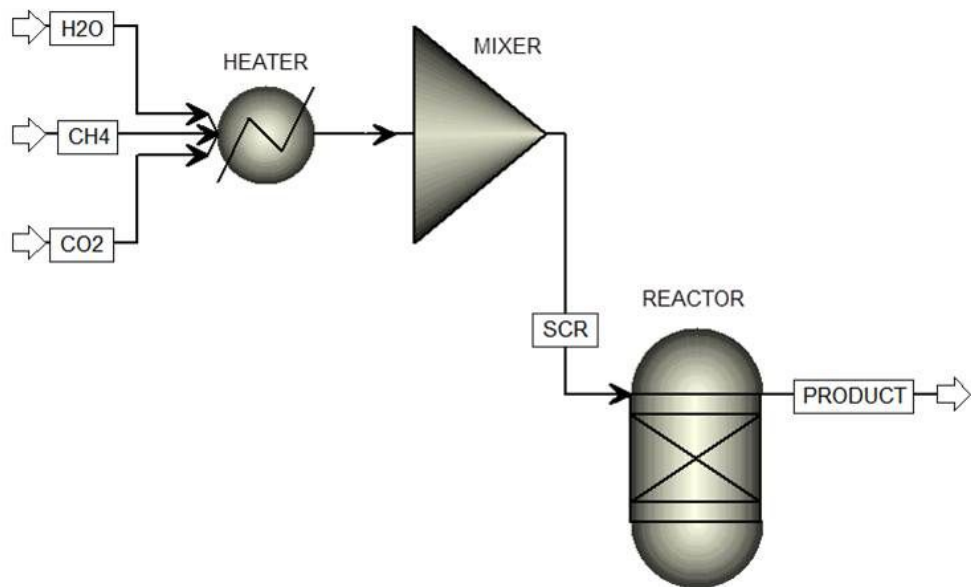


Fig. 7. Flow diagram for modeling a SCR reactor by ASPEN Plus

Table 2. Simulation results estimated by ASPEN plus in the SCR of methane

Feed molar rate (kmol/h)			Product molar ratio (kmol/h)					CH ₄ conv. (%)	CO ₂ conv. (%)	H ₂ /CO ratio
CH ₄	H ₂ O	CO ₂	H ₂	CO	H ₂ O	CO ₂	CH ₄			
100	180	90	267.8	130.6	111.4	59.0	0.4	99.6	41.0	2.05
100	190	90	270.2	128.3	119.0	61.4	0.4	99.6	38.6	2.11
100	200	90	272.6	126.0	126.7	63.6	0.3	99.7	36.4	2.16
100	180	100	263.4	135.1	115.8	64.5	0.4	99.6	35.5	1.95
100	190	100	265.9	132.7	123.4	66.9	0.3	99.7	33.1	2.00
100	200	100	268.3	130.4	131.1	69.2	0.3	99.7	30.8	2.06
100	180	110	259.2	139.4	120.1	70.2	0.3	99.7	29.8	1.86
100	190	110	261.7	137.0	127.7	72.6	0.3	99.7	27.4	1.91
100	200	110	264.1	134.7	135.3	75.0	0.3	99.7	25.0	1.96

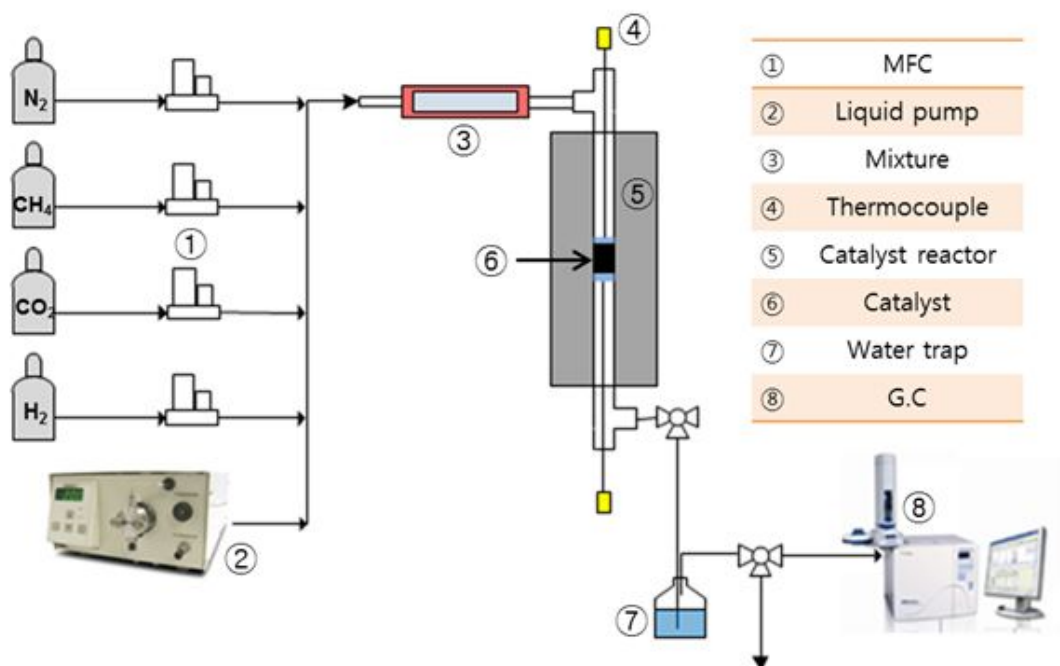


Fig. 8. Experimental setup for the steam-CO₂ reforming of methane

3.6. γ -Al₂O₃/Ni foam characterization

Fig. 9 shows SEM image of the bare and wash-coated Ni foam. The bare Ni foam gas boundary layers between the lattices as shown in Fig. 9 (b), whereas the boundary layer was not observed at the wash-coated Ni foam as shown in Fig. 9 (d). This means that the γ -Al₂O₃ wash-coat layer was well deposited on the surface of the Ni foam. The γ -Al₂O₃ layer was uniform on the entire Ni foam, as shown in Fig. 9 (c).

Fig. 10 shows the XRD patterns at different calcination temperatures. The calcination temperature was varied from 600 to 900°C. The NiO and Al₂O₃ peaks were only observed, and the peak intensity increased with increasing temperature. The NiO peaks of 37°, 43° and 62° were observed at all temperature. Therefore, Ni/Al₂O₃ catalysts on the metallic foam were well established after performing the coating process proposed in the present study. However, weak intensity NiO peak at 75° was observed at 800 and 900°C. In general, high calcination temperature enhances the crystallite growth and particle sintering, which results in faster growth speed at higher calcination temperature [51]. The NiO peak at 75° was appeared at high calcination temperature > 800°C: however, at temperatures < 800°C, the peak intensity was too weak to be identified clearly. The particle size of NiO was calculated using Scherrer's equation, and is shown in Table 3. The NiO particle size increased with increasing calcination temperature. A large particle size caused the low dispersion of the Ni catalyst on the Al₂O₃, resulting in low catalytic activity [52].

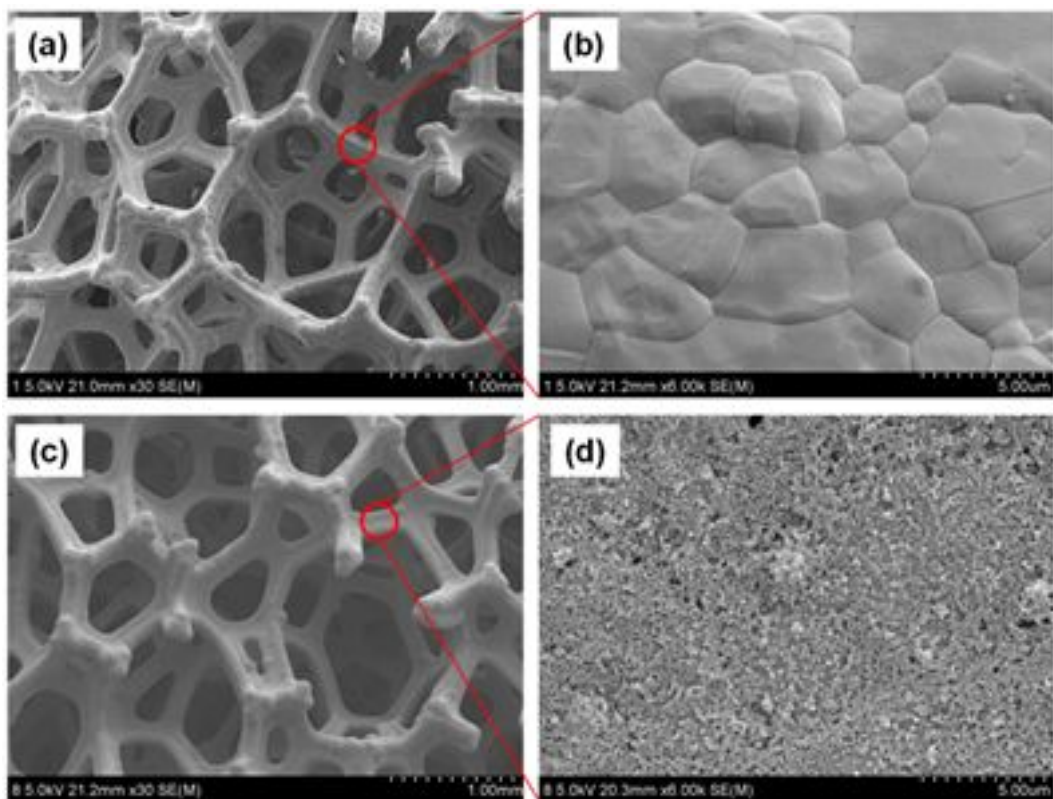


Fig. 9. SEM images of the Ni/ γ -Al₂O₃/Ni foam: bare Ni foam (a) $\times 30$, (b) $\times 6000$, and Ni/ γ -Al₂O₃/Ni foam (c) $\times 30$, and (d) $\times 6000$.

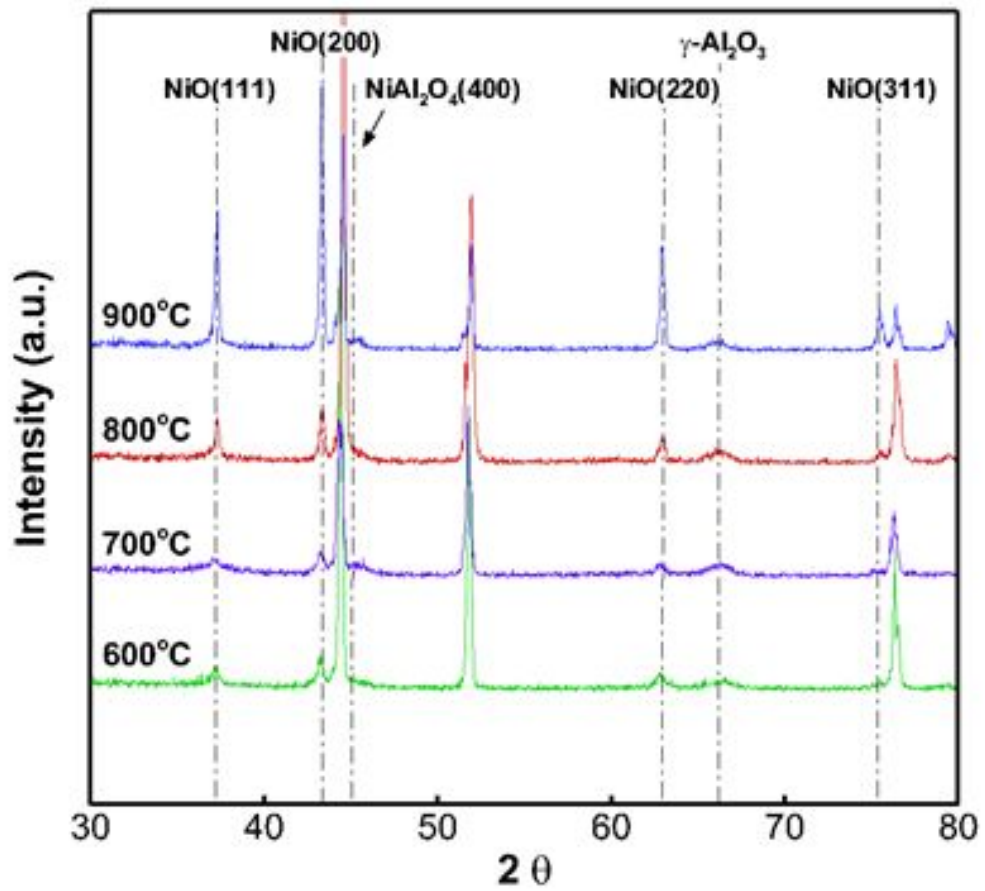


Fig. 10. XRD patterns of the Ni/γ-Al₂O₃/Ni foam at the different calcination temperature

Table 3. Particle size of the Ni/ γ -Al₂O₃/Ni foam catalyst after the calcination.

Calcination temperature (°C)	NiO (111) particle size (nm)	NiO (220) particle size (nm)
600	-	2.68
700	3.12	2.68
800	12.46	4.26
900	12.46	8.56

3.7. Surface quality of the wash-coated catalyst

Table 4 lists the number of wash-coating repetitions and the weight fraction of the wash-coat according to the $\text{Al}_2\text{O}_3/\text{AIP}$ molar ratio. The coating was repeated for all samples to be an equal weight fraction to ~ 20 wt.%. When the $\text{Al}_2\text{O}_3/\text{AIP}$ molar ratio was 1, the coating was repeated 13 times. On the other hand, only 2 coatings were sufficient to obtain the same weight fraction when the $\text{Al}_2\text{O}_3/\text{AIP}$ molar ratio was 9. This is because the viscosity of the coating sol increased with increasing $\text{Al}_2\text{O}_3/\text{AIP}$ molar ratio. Fig. 11 shows the weight fraction of the Al_2O_3 wash-coat layer to the Ni foam as a repetition of the wash-coating. The weight fraction of the Al_2O_3 wash-coat layer per wash-coating increased with increasing $\text{Al}_2\text{O}_3/\text{AIP}$ molar ratio. When a high $\text{Al}_2\text{O}_3/\text{AIP}$ molar ratio was used, the number of repetitions of the wash-coating can be reduced to obtain the desired weight fraction of the catalyst to the Ni foam. If 20 wt.% $\text{Al}_2\text{O}_3/\text{Ni}$ foam is required, e.g. 13 times, the wash-coating should be repeated with a $\text{Al}_2\text{O}_3/\text{AIP}$ molar ratio of 1.0. The weight fraction of Al_2O_3 wash-coat increased in direct proportion to the number of wash-coatings. The average increase of the weight fraction at $\text{Al}_2\text{O}_3/\text{AIP}$ ratio of 1.0 was 1.46 wt.% per wash-coating. The $\text{Al}_2\text{O}_3/\text{AIP}$ molar ratio should be increased by 5.0 to obtain a 20 wt.% $\text{Al}_2\text{O}_3/\text{Ni}$ foam within 7 wash-coatings. Fig. 12 presents SEM images showing the coating quality of the wash-coat layers when the coating was performed using the wash-coating sol at different $\text{Al}_2\text{O}_3/\text{AIP}$ molar ratios. The as-prepared samples have no cracks on the surface and the aggregation of catalyst particles. Cracks formed after calcining at 800 °C. The wash-coat peeled off from the Ni foam at an $\text{Al}_2\text{O}_3/\text{AIP}$ molar ratio of <5 because it shrank as the AIP was being decomposed during calcination. The wash-coat was seriously cracked at an $\text{Al}_2\text{O}_3/\text{AIP}$ molar ratio of >5 because the aggregated Al_2O_3 particles were coated thick on the surface of the Ni foam. The catalyst layer coated with an $\text{Al}_2\text{O}_3/\text{AIP}$ molar ratio of 5 had no cracks after calcination.

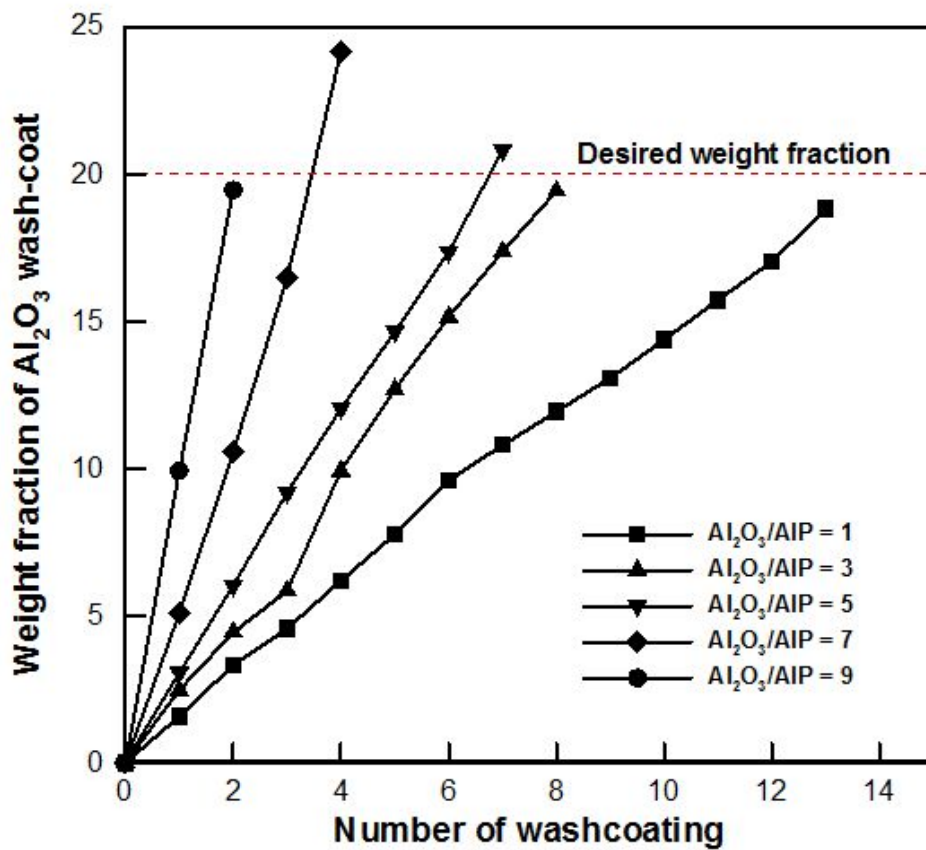


Fig. 11. Weight fraction of the Al_2O_3 wash-coat layer to a Ni foam as a function of the number of wash-coatings.

Table 4. Number of wash-coating repetitions to obtain ~20 wt.% of wash-coat according to the $\text{Al}_2\text{O}_3/\text{AIP}$ molar ratio.

	$\text{Al}_2\text{O}_3/\text{AIP}$ molar ratio				
	1	3	5	7	9
Number of coating repetition	13	8	7	4	2
Wight fraction of wash-coat (wt.%)	18.81	19.42	20.80	24.13	19.45

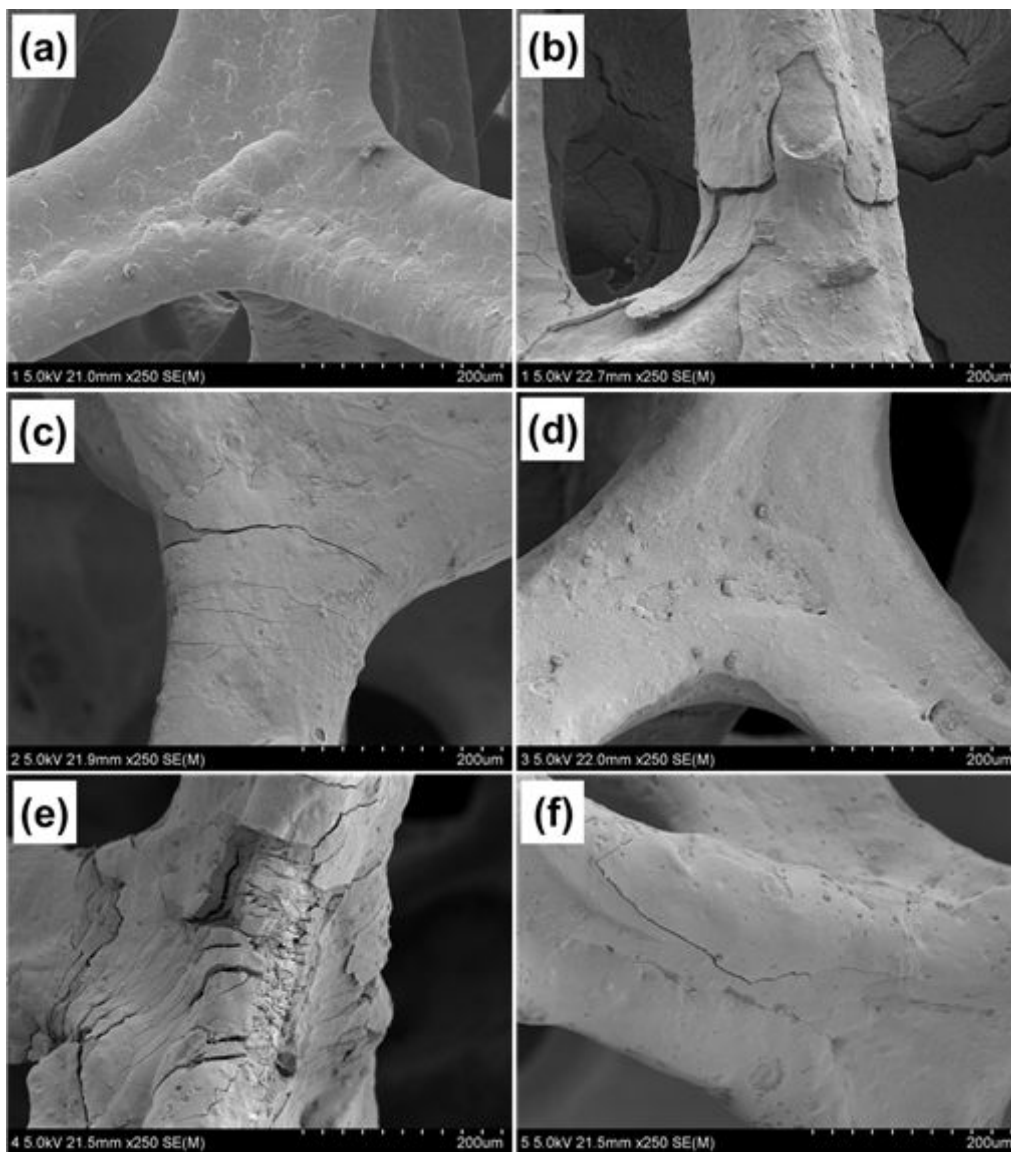


Fig. 12. SEM images of the wash-coat layer at different $\text{Al}_2\text{O}_3/\text{AIP}$ molar ratios: (a) bare Ni foam, (b) $\text{Al}_2\text{O}_3/\text{AIP}=1$, (c) $\text{Al}_2\text{O}_3/\text{AIP}=3$, (d) $\text{Al}_2\text{O}_3/\text{AIP}=5$, (e) $\text{Al}_2\text{O}_3/\text{AIP}=7$, and (f) $\text{Al}_2\text{O}_3/\text{AIP}=9$.

3.8. Adhesion strength of the wash-coated catalyst

Table 5 lists the fall-off rate of the wash-coated Ni foams with different $\text{Al}_2\text{O}_3/\text{AIP}$ molar ratios after 10 and 50 h. During the fall-off test for 10 h, the weight loss of the wash-coat layer was 0.96% in the case of a $\text{Al}_2\text{O}_3/\text{AIP}$ ratio of 5. In other cases ($\text{Al}_2\text{O}_3/\text{AIP} = 1, 3, 7$ and 9), the weight loss was greater than 1.0%. After 50 h, the weight loss was the highest at an $\text{Al}_2\text{O}_3/\text{AIP}$ ratio of 3, whereas the weight loss was less than 2.0% in others. The weight loss in cases of an $\text{Al}_2\text{O}_3/\text{AIP}$ ratio of 7 and 9 occurred mostly within 10 h. After 50 h, however, the weight loss was relatively low because the weight losses were similar to the case of an $\text{Al}_2\text{O}_3/\text{AIP}$ ratio of 5. That is because cracks formed on the wash-coating in cases of an $\text{Al}_2\text{O}_3/\text{AIP}$ ratio of 7 and 9, and the cracked wash-coat layers fell off after 10 h. After the cracked layers were removed from the Ni foam, the remaining wash-coat layer showed low weight loss after 50 h. Considering the fall-off test and SEM images, the optimal $\text{Al}_2\text{O}_3/\text{AIP}$ ratio was determined to be 5 because of the uniform surface without cracks and the lowest fall-off rate.

Table 5. Fall-off rate of the wash-coated Ni foams with different $\text{Al}_2\text{O}_3/\text{AIP}$ molar ratios.

	$\text{Al}_2\text{O}_3/\text{AIP}$ molar ratio				
	1	3	5	7	9
Weight loss (%) After 10 hours	1.00	1.47	0.96	1.42	1.44
Weight loss (%) After 50 hours	1.98	2.45	1.91	1.90	1.92

3.9. Heat transfer characteristics of the wash-coated catalyst

Fig. 13 shows the Nusselt numbers of the reactor packed with γ -Al₂O₃ pellets and the wash-coated Ni foam, respectively. The Nusselt number of the wash-coated Ni foam was higher than that of the γ -Al₂O₃ pellets over the entire range of flow rates. The improvement in the heat exchange rate of the Ni foam, which means the difference in the Nusselt number between the Ni foam and pellets, increased with increasing flow rate. Fig. 14 shows the inlet and outlet temperatures as a function of the flow rate at the γ -Al₂O₃/Ni foam and γ -Al₂O₃ pellets. The temperature difference between the inlet and outlet became large through the reactor as the flow rate was increased. On the other hand, the temperature difference of the γ -Al₂O₃/Ni foam was much lower than that of the γ -Al₂O₃ pellets. Furthermore, the outlet temperature of the γ -Al₂O₃/Ni foam was maintained for gas feeding. This means that the wash-coated Ni foam has a more uniform temperature distribution along the reactor.

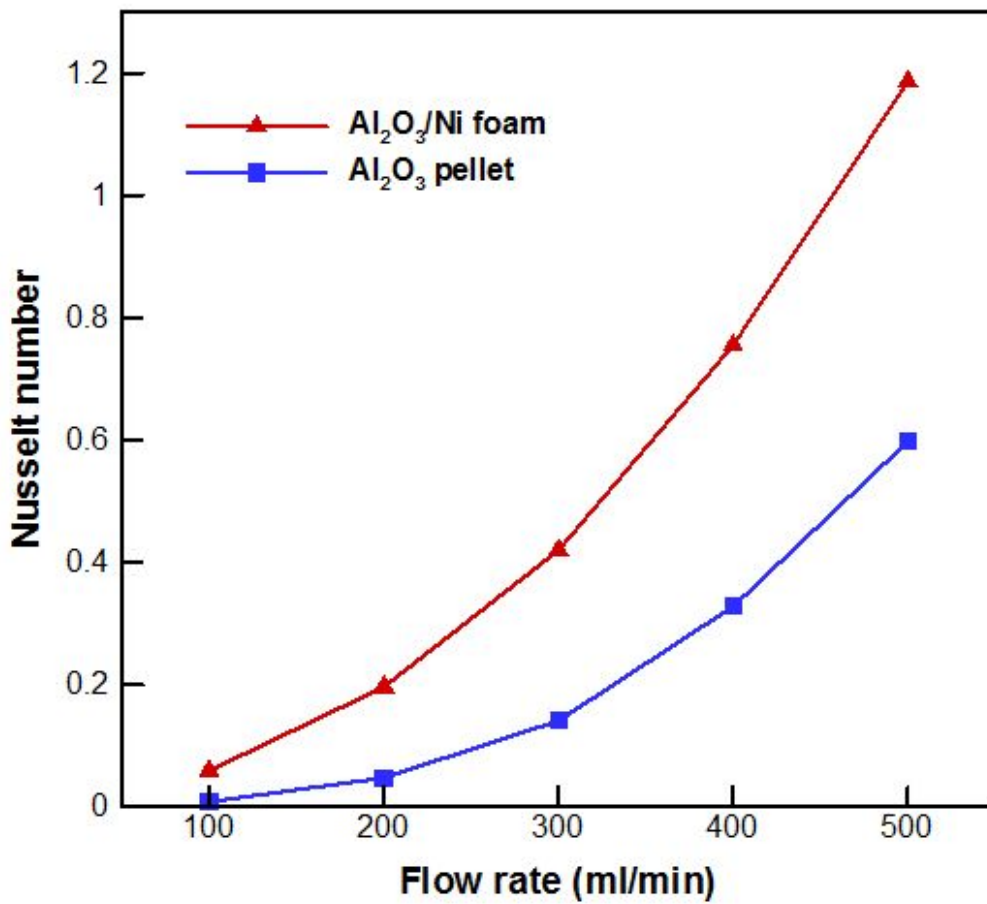


Fig. 13. Nusselt numbers of the reactor packed with the $\gamma\text{-Al}_2\text{O}_3$ pellets and wash-coated Ni foam

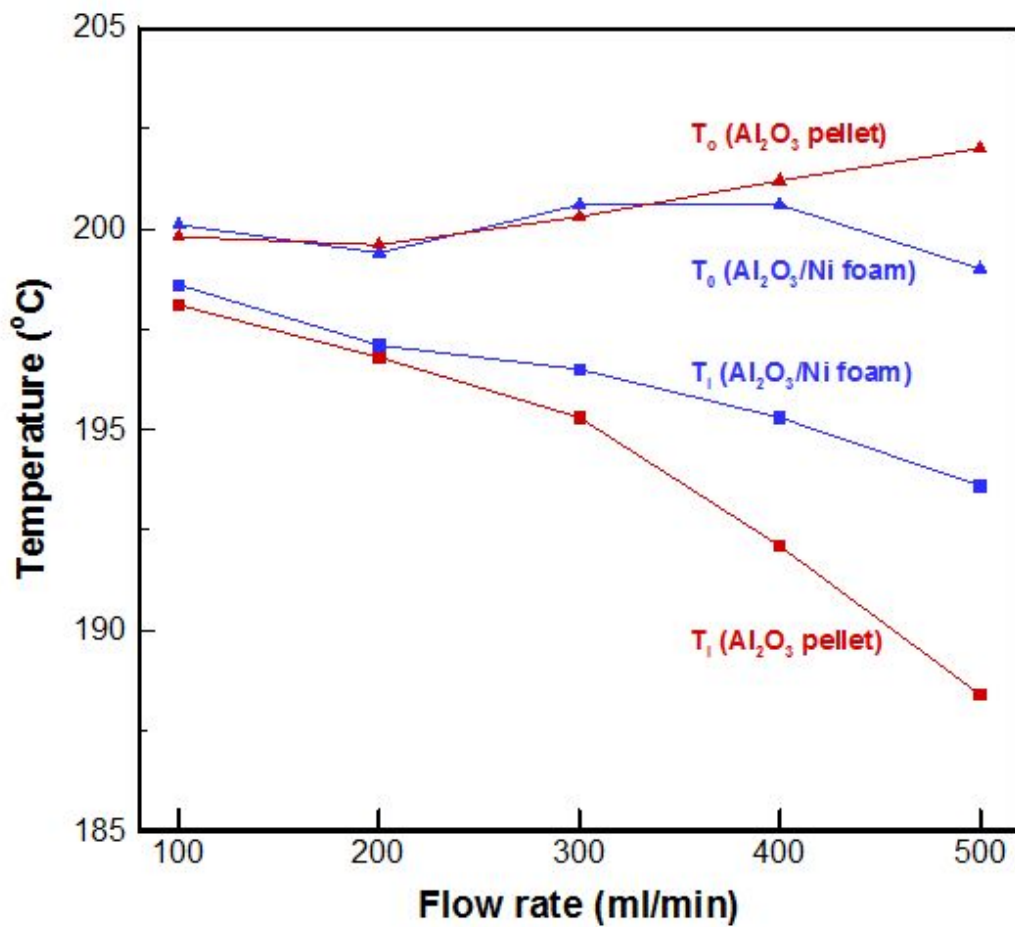


Fig. 14. Inlet and outlet temperatures as a function of the flow rate at the $\gamma\text{-Al}_2\text{O}_3/\text{Ni}$ foam and $\gamma\text{-Al}_2\text{O}_3$ pellets.

3.10. Comparison of the Ni/ γ -Al₂O₃/Ni foam with the Ni/ γ -Al₂O₃ pellet catalyst

Fig. 15 shows the CH₄ and CO₂ conversions of the pellet and Ni foam catalysts as a function of temperature. The reaction temperature was varied from 450 to 950°C at a space velocity of 10,000 h⁻¹. The CH₄ conversion of both catalysts increased with increasing temperature; however, the CH₄ conversion of the Ni foam catalyst was much higher than that of the pellet catalyst at the entire temperature range, as shown in Fig. 15 (a). Similarly, the CO₂ conversions increased with increasing temperature, and the CO₂ conversion of the Ni foam catalyst was higher than that of the pellet catalyst at temperatures higher than 642°C, as shown in Fig. 15 (b). Fig. 16 shows the temperature difference between the inlet and outlet of pellet and Ni foam catalysts, respectively. The temperature difference of the Ni foam catalyst was lower than that of the pellet catalyst. The Ni foam catalyst has a good thermal dispersion over the catalyst surface because it has higher thermal conductivity than the pellet catalyst. Therefore, the Ni foam catalyst has a uniform temperature distribution throughout the entire catalyst region. On the other hand, the pellet catalyst had appreciable temperature difference between the catalyst inlet and outlet. The difference in temperature between the pellet and Ni foam catalyst would be not considerable in a small-scale reactor but the Ni foam catalyst will be more effective when the reactor size and space velocity are increased.

The temperature of the catalyst outlet was lower than that of the catalyst inlet because the SCR is an endothermic reaction. The outlet of the Ni foam catalyst, however, had temperature higher than the inlet at temperatures >642°C. It means that the endothermic reaction took place at the front of the catalyst. If more reactants were fed, the temperature would be more uniform because the reaction takes place through the entire catalyst. In the other words, the Ni foam catalyst is more effective at a high space velocity than the pellet catalyst.

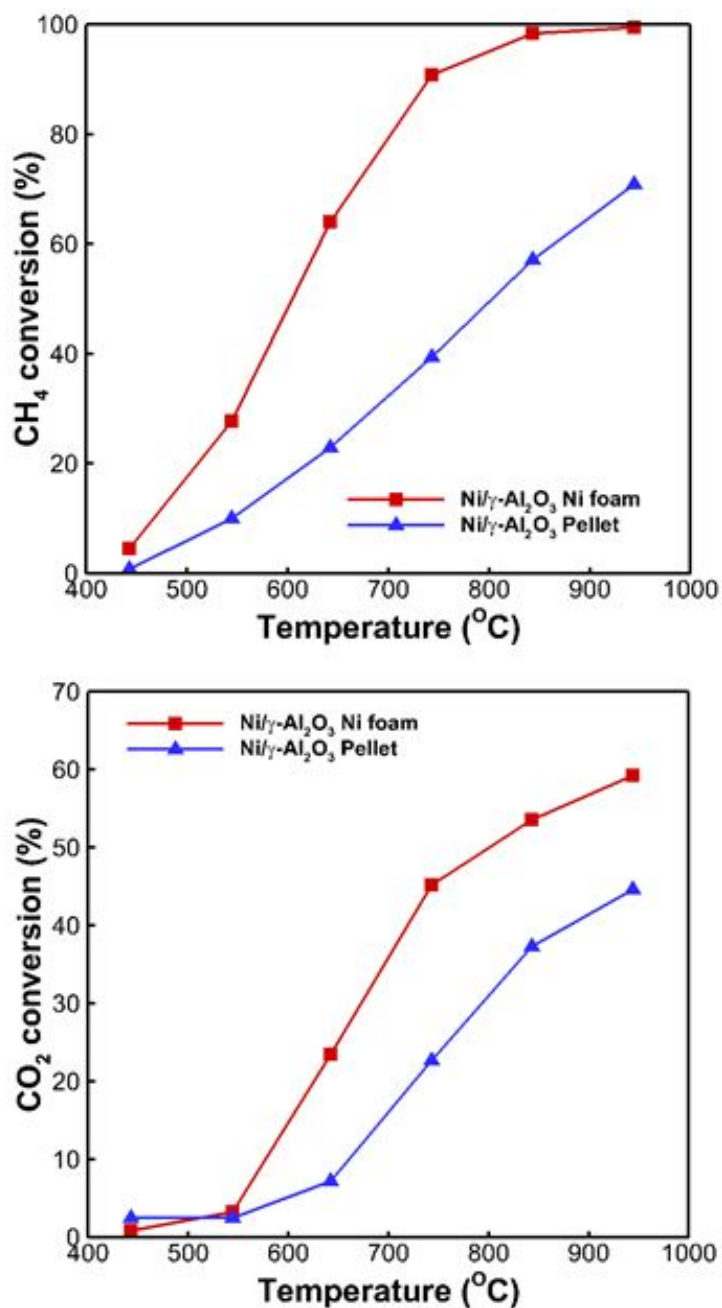


Fig. 15. CH₄ and CO₂ conversions of the pellet and metallic foam catalyst as a function of temperature at a space velocity of 10,000h⁻¹

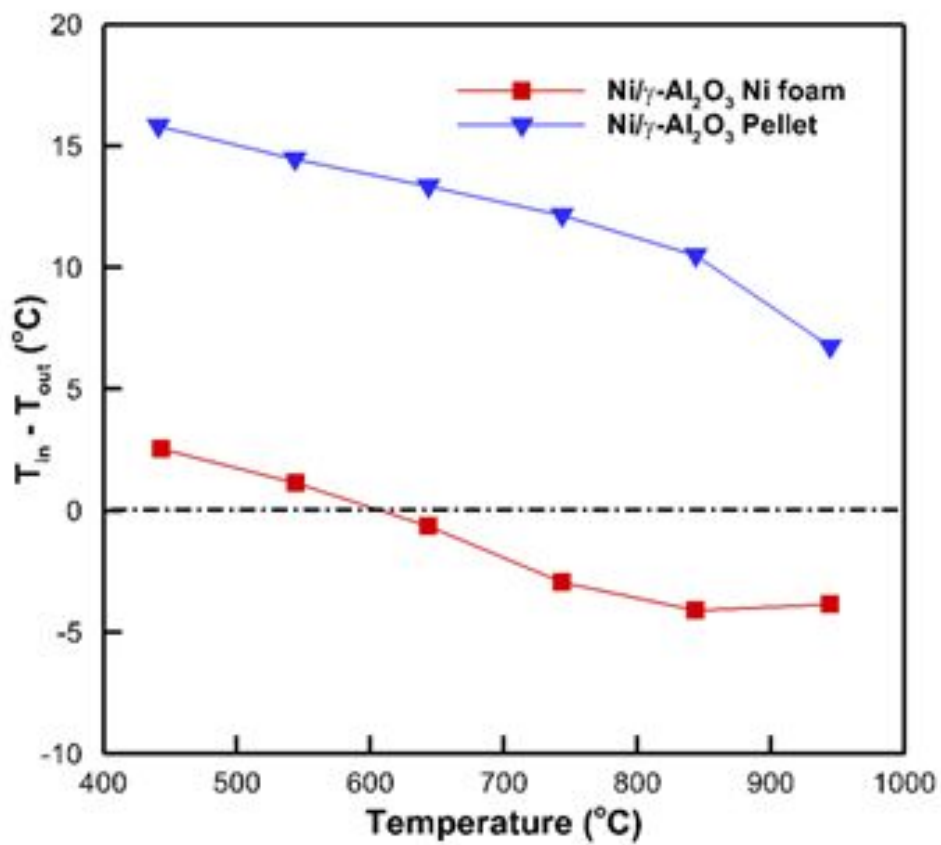


Fig. 16. Temperature difference between the inlet and outlet of the pellet and Ni foam catalysts

3.11. Effect of temperature on the reactivity of the Ni/ γ -Al₂O₃/Ni foam catalyst

As aforementioned, the CH₄ and CO₂ conversions increased with increasing temperature as shown in Fig. 15. CH₄ conversion was 64.0% at 642°C, whereas it reached more than 90.0% at 743°C. CH₄ conversion of >98.0% was almost achieved at 843 °C. CO₂ conversion was 23.5% at 642°C, and increased gradually with increasing temperature. CO₂ conversion was 53.6% at 843°C. The syngas production rate increased with increasing temperature because CH₄ conversion also increased as shown in Fig. 17 (a). The molar ratio of syngas (H₂/CO) decreased with increasing temperature as shown in Fig. 17 (b). The H₂/CO molar ratio should be adjusted to 1.8–2.0 for GTL-FPSO application with Co-based FT synthesis. The H₂/CO molar ratio was approximately 2.0 at 850 °C. Lee et al. calculated the H₂/CO molar ratio of the SCR reaction as the temperature varied using chemical equilibrium. They resulted that the H₂/CO molar ratio can be adjusted to 2.0 at 800°C with the feed ratio of CH₄:H₂O:CO₂ = 1:2:1. Our experimental result shows an agreement with their calculation.

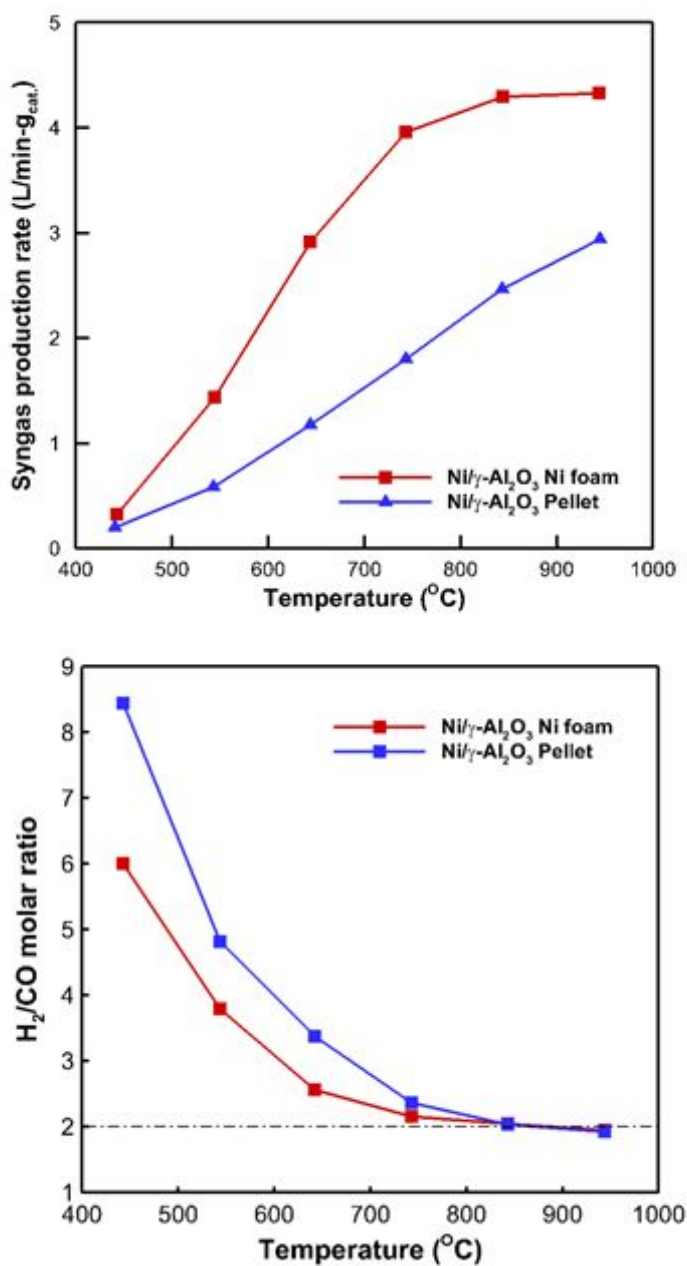


Fig. 17. Syngas production rate and H₂/CO molar ratio of the pellet and metallic foam catalyst as a function of temperature at a space velocity of 10,000h⁻¹.

3.12. Effect of space velocity on the reactivity of the Ni/ γ -Al₂O₃/Ni foam catalyst

Fig. 18 shows the CH₄ conversion of the Ni/ γ -Al₂O₃/Ni foam catalyst as a function of the space velocity at 700 and 800°C, respectively. CH₄ conversion decreased with increasing space velocity at both temperatures. On the other hand, the degree of the decrease was considerable at 700°C compared to 800°C. This is because the temperature gradient in the reactor becomes large as the space velocity is increased from 700°C. At the space velocity of 40,000 h⁻¹, the CH₄ conversion was >95% at 800°C, which is considerably high compared to existing pellet catalysts. The solid line in Fig. 18 represents a linear plot of the experimental data. At space velocities >100,000 h⁻¹, the CH₄ conversion might be >90% at 800°C. This verification is under progress using a scale-up reactor.

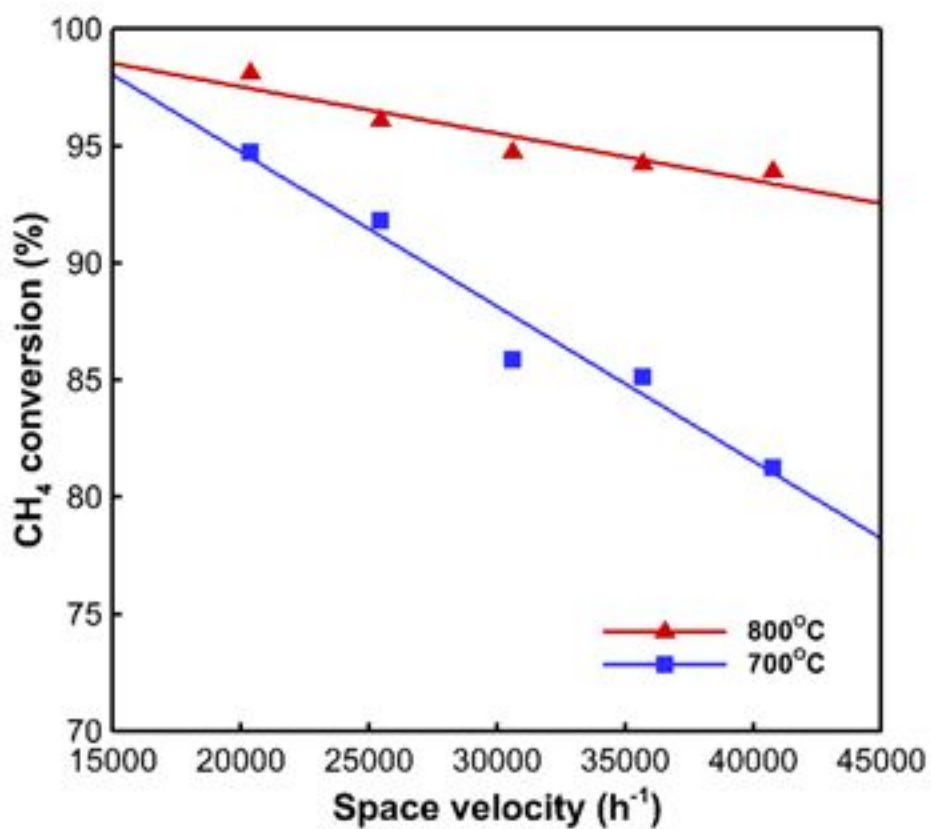


Fig. 18. CH₄ conversion of the Ni/γ-Al₂O₃/Ni foam catalyst as a function of the space velocity at 700 and 800°C.

3.13. Catalytic activity of the wash-coated catalyst

The simulation of the SCR reaction was performed by using ASPEN Plus Simulation including the product molar ratio, CH_4 and CO_2 conversion, and H_2/CO molar ratio at various feed compositions. The H_2/CO molar ratio was adjusted to 2.0 when the $\text{CH}_4:\text{H}_2\text{O}:\text{CO}_2$ composition was 1.0:1.9:1.0. A previous experimental study reported that the H_2/CO molar ratio decreased slightly because CO_2 conversion increased more than the simulated value. The H_2/CO molar ratio could be adjusted to 2.0 by increasing the H_2O supply. Therefore, the feed composition selected was $\text{CH}_4:\text{H}_2\text{O}:\text{CO}_2 = 1.0:2.0:1.0$ in the present study. At this feed composition, the conversions of CH_4 and CO_2 were 99.7% and 30.8%, respectively.

Fig. 19 shows the CH_4 and CO_2 conversions of the bare Al_2O_3 , bare Ni foam, $\text{Al}_2\text{O}_3/\text{Ni}$ foam and $\text{Ni}/\text{Al}_2\text{O}_3/\text{Ni}$ foam. First, there was no conversion in the empty reactor, which means that a homogeneous reaction did not occur. On the other hand, the bare Al_2O_3 and bare Ni foam showed reactivity even if the Ni catalyst was not loaded, and the bare Ni foam showed slightly higher CH_4 conversion than the bare Al_2O_3 . In general, the Ni foam plays the role of a structuring material for the catalysts to improve heat and mass transfer of the catalyst bed in the reactor. The Ni foam could also have reactivity (CH_4 conv. = 18.9%, CO_2 conv. = 10.2%) because Ni is active on the SCR reaction. After wash-coating the Al_2O_3 layer on the Ni foam, the CH_4 and CO_2 conversions increased by 69.1% and 34.0% compared to the bare Ni foam. These conversions were higher than those of the bare Al_2O_3 , bare Ni foam and their combinations. This is because a small amount of Ni nitrate was contained in the wash-coating sol coated over the surface of the Ni foam. Ni nitrate could be formed by nitric acid that was added to adjust the pH of the wash-coating sol. After the Ni catalyst was coated, the $\text{Ni}/\text{Al}_2\text{O}_3/\text{Ni}$ foam showed high reactivity: the CH_4 and CO_2 conversions were 99.7% and 44.0%, respectively. Fig. 20 shows the syngas flow rate and H_2/CO molar ratio of the bare Al_2O_3 bead, bare Ni foam, $\text{Al}_2\text{O}_3/\text{Ni}$ foam and $\text{Ni}/\text{Al}_2\text{O}_3/\text{Ni}$ foam. The syngas flow rate showed a similar tendency to the CH_4 and CO_2

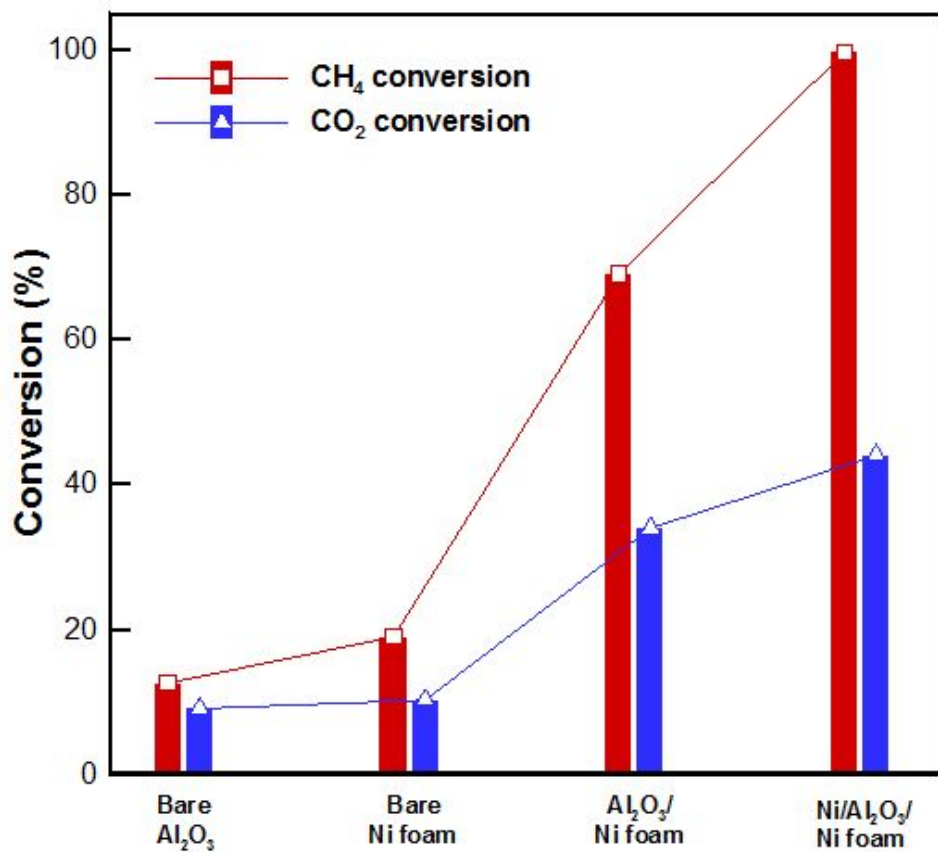


Fig. 19. CH₄ and CO₂ conversion of the bare Al₂O₃ bead, bare Ni foam, Al₂O₃/Ni foam, and Ni/Al₂O₃/Ni foam.

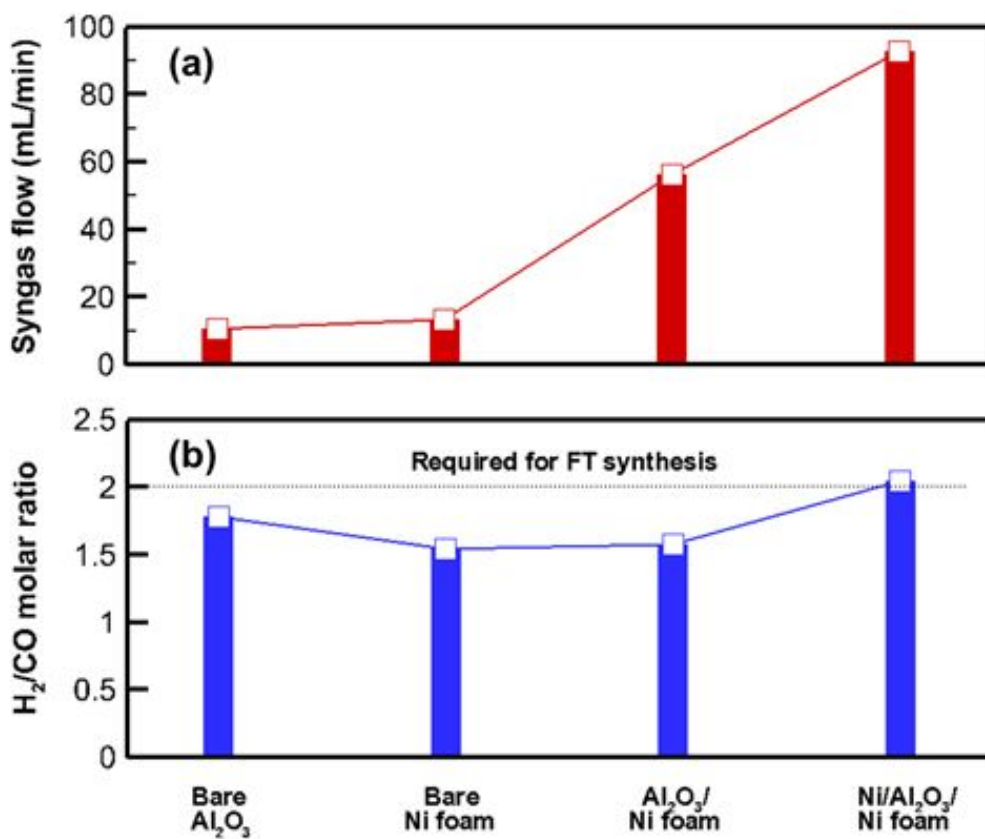
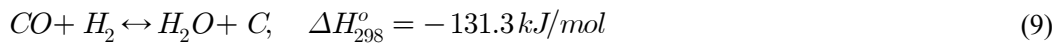
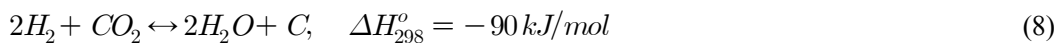
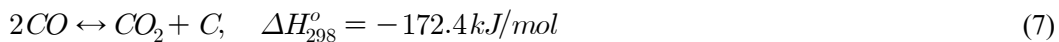


Fig. 20. (a) Syngas flow rate ($\text{H}_2 + \text{CO}$) and (b) H_2/CO molar ratio of the bare Al_2O_3 bead, bare Ni foam, $\text{Al}_2\text{O}_3/\text{Ni}$ foam, and $\text{Ni}/\text{Al}_2\text{O}_3/\text{Ni}$ foam.

3.14. long-term durability of the Ni/ γ -Al₂O₃/Ni foam catalyst

In GTL-FPSO applications, it is difficult that the frequent replacement of the catalyst. Therefore, the catalyst durability is more important for GTL-FPSO applications compared to the conventional GTL process. Fig. 21 shows the results of the durability test of the Ni/ γ -Al₂O₃/Ni foam catalyst. The durability test was performed at a high space velocity of 130,000 h⁻¹ for 50 h, because the conversions are high at low space velocities and the durability test time is very time-consuming. The CH₄ and CO₂ conversions were 75% and 20% when the reaction was initiated. The conversions decreased gradually 25 h after initiating the reaction. The conversions were reduced by 10% after the test for 50 h. The performance degradation of the catalyst was caused by two reasons: one is carbon formation and the other is crack formation. The carbon was formed on the active sites of the catalyst as the contact time of the reactants with the catalysts was increased (low space velocity). It reported that the carbon formation can be reduced by increasing the space velocity because radicals formed on the catalyst surface easily desorb from the catalyst surface. In the long-term reaction of the metallic foam catalyst, however, the total carbon formation during the reaction was 58.3 mg/g-cat. h. This amount was relatively high compared to the powdered catalyst in the literature [00] even if the reaction was performed at a higher space velocity. The metallic foam catalyst has a relatively larger void volume in the catalyst bed, so that the flow boundary layer on the surface of the catalyst is thicker than the powdered catalyst. Thus, the radical desorption from the catalyst surface was relatively less effective on the metallic foam catalyst. Moreover, cold-spots could occur locally in the metallic foam catalyst due to the high space velocity. Consequently, the carbon formation increased during the long-term reaction at the high space velocity. The carbon was formed by the Boudouard reaction (Eq. (7)), CO₂ hydrogenation (Eq. (8)), and CO hydrogenation (Eq. (9)). Among these, the Boudouard reaction is the most thermodynamically favorable at temperature lower than the reforming temperature (~800 °C).



The catalyst durability could be deteriorated by crack formation. Fig. 22 shows SEM images of the catalyst after the durability test. The cracks were on the micro scale after the durability test for 50 h but would be expected to increase in size as the reaction was continued. The crack formations were due to the different thermal expansion coefficient between the Al_2O_3 layer and Ni foam. The thermal expansion coefficient of the Ni (12.5×10^{-6} 1/K) was 1.47 times higher than that of Al_2O_3 (8.5×10^{-6} 1/K). Consequently, the catalyst can peel off during the long-term reaction, resulting in a deterioration of the catalyst performance. The adhesion of the catalyst layer on the metallic foam will be improved by adding an alternative bonding agent as a future work.

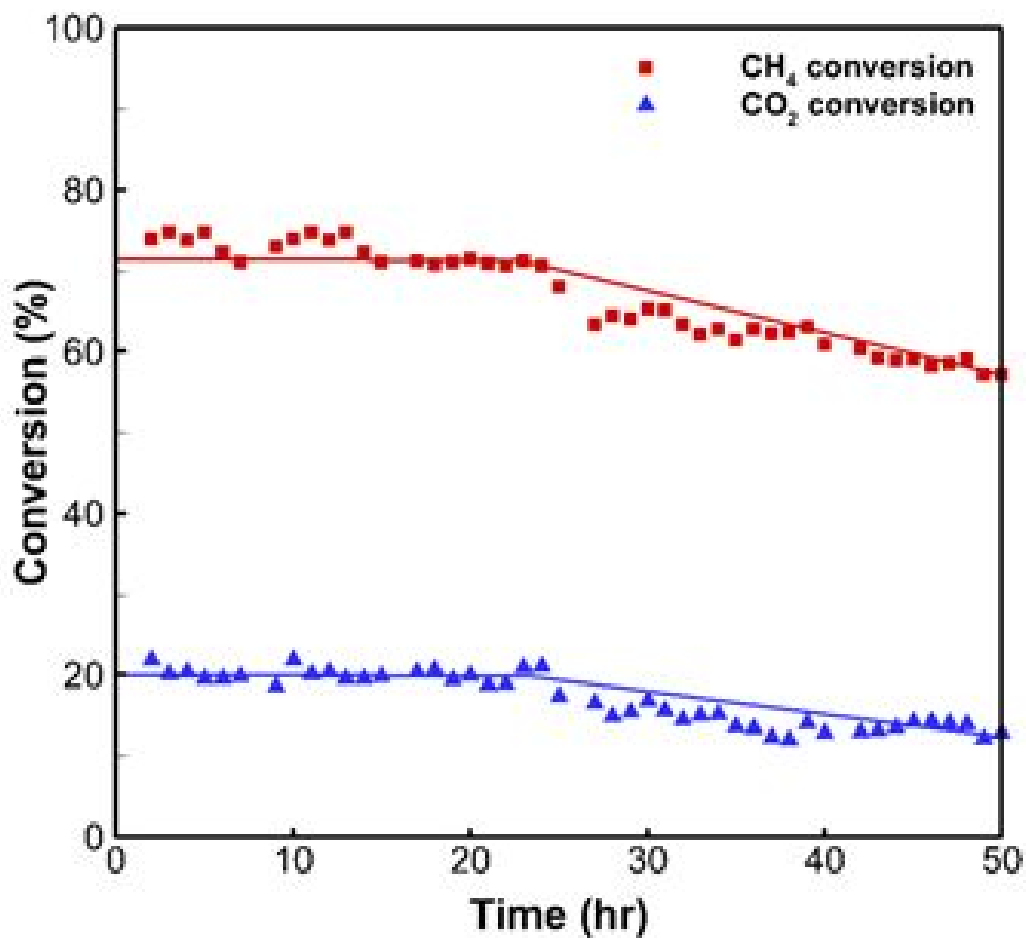


Fig. 21. Result of the durability test of the Ni/ γ -Al₂O₃/Ni foam catalyst at 800°C for 50 h at a space velocity of 130,000 h⁻¹.

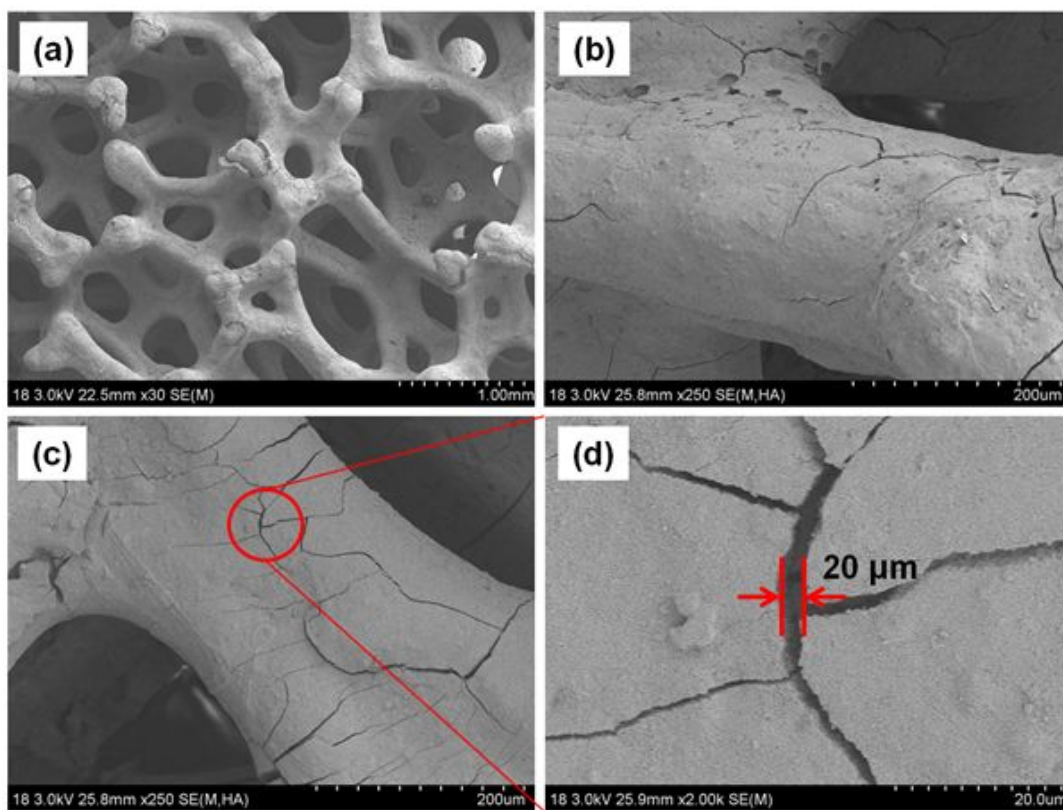


Fig. 22. SEM images of the Ni/ γ -Al₂O₃/Ni foam catalyst after the durability test: (a) $\times 30$, (b) and (c) $\times 250$, and (d) $\times 2000$.

Chapter 4. Perovskite-type catalysts (Polyol method)

4.1. Preparation of perovskite type catalyst

The perovskite type catalysts, $\text{La}_{0.8}\text{Sr}_{0.2}\text{NiO}_3$ were prepared by sol-gel method and EDTA cellulose method. PVA (Alfa Aesar Co.), PAA (Sigma- Aldrich) and EDTA (Samchun pure chemical Co.) were dissolved in distilled water that is heated at 65°C for 30 min, respectively. Perovskite-type catalysts were prepared by a polyol method. PVP (average molecular weight, $M_w = 10,000$; Junsei Chemical Co., Ltd., Japan) was used as a gelation agent and polymer stabilizer, which was dissolved with ethylene glycol (EG; Duksan Pure Chemicals Co., Ltd., Korea) in distilled water that was heated to 65°C, and the mixture was stirred until complete dissolution. Since we were examining the effects of concentration, the PVP molarity varied from 0.5 to 5.0 M, and the amount of EG remained constant. Three nitrates, $\text{La}(\text{NO}_3)_3$, $\text{Sr}(\text{NO}_3)_2$, and $\text{Ni}(\text{NO}_3)_2$ (Samchun Pure Chemical Co., Ltd., Korea) were dissolved in the PVP/EG solution by stirring. After the solution was evaporated at 80°C on a hot plate for 3 h, the perovskite sol was rapidly cooled in a freezer until the gel was obtained. The gel was then dried in a convection oven at 100°C for a day. After drying, the perovskite gel was pre-calcined in air at 300°C for 2 h to remove nitrate components in the perovskite gel. Afterwards, the temperature was raised to 800°C at 2.5°C/min, and it was calcined again for 5 h, which yielded a $\text{La}_{0.8}\text{Sr}_{0.2}\text{NiO}_3$ perovskite-type catalyst in the powdered state.

In general, perovskite-type catalysts have been employed in the powdered state for reforming reactions [53]. Coating of the catalyst on supports makes it possible to use it in various applications [54]. The powdered perovskite-type catalysts were coated onto $\alpha\text{-Al}_2\text{O}_3$ spherical supports using a physical method, in which a ball-mill process was performed for 3 days in a container at a fixed speed of 270 rpm. The weight fraction of the catalyst to the support was adjusted to 3.0 ± 0.3 wt.%, as shown in Fig. 23.

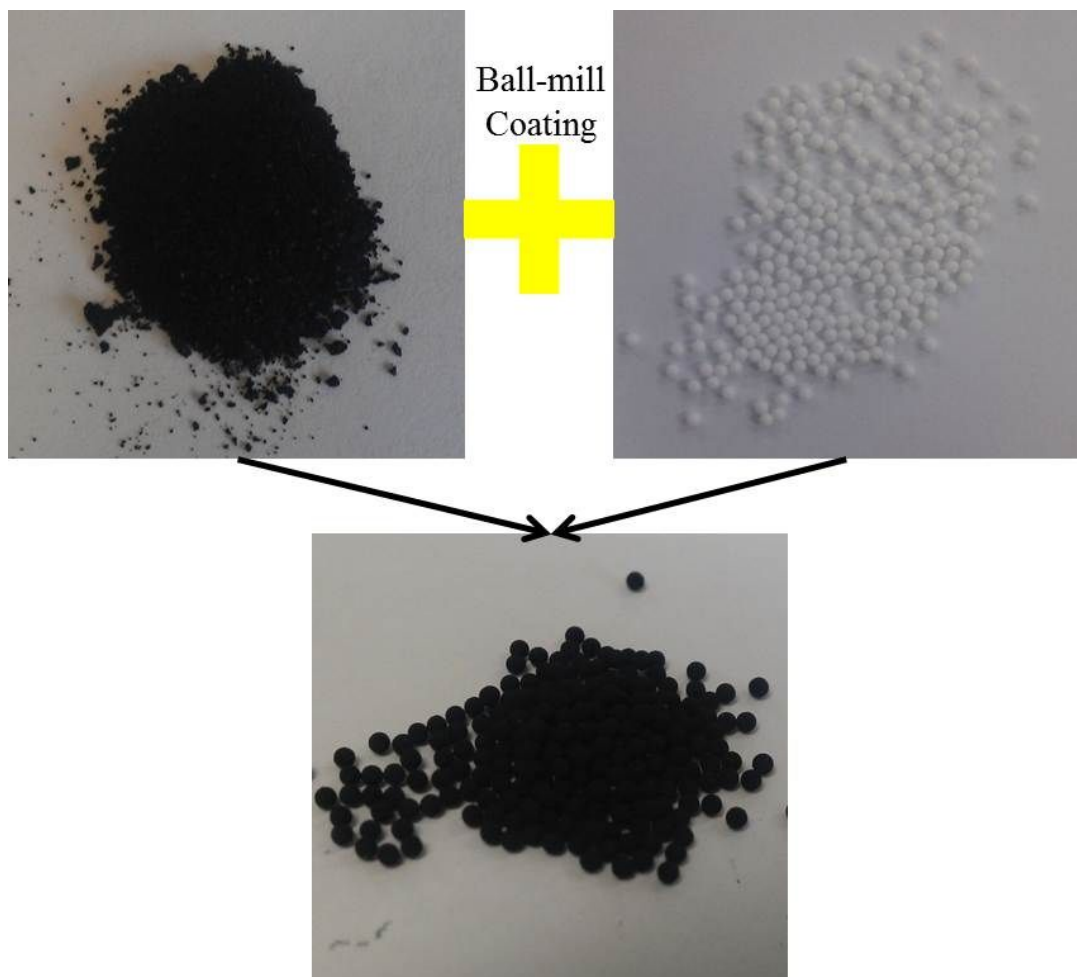


Fig. 23. $\text{La}_{0.8}\text{Sr}_{0.2}\text{NiO}_3/\alpha\text{-Al}_2\text{O}_3$ catalyst:

4.2 Characterization of perovskite type catalyst

The catalysts before and after the reaction were characterized by different analytical techniques, such as X-ray diffraction (XRD), field emission scanning electron microscopy (FESEM), H₂-temperature programmed reduction (H₂-TPR), Fourier transform infrared spectrometry (FT-IR) and Thermogravimetric analysis (TGA).

4.2.1. H₂-temperature programmed reduction (H₂-TPR)

H₂- temperature programmed reduction (H₂-TPR) analysis was performed to investigate the reducibility of catalysts using a chemisorption analyzer (BELCAT; BEL Japan, Inc.) equipped with a thermal conductivity detector. We packed 35 – 50 mg of catalysts into a reactor, and a 5% H₂/Ar gas mixture was supplied at a flow rate of 50 mL/min. The TPR profiles were obtained by increasing the temperature at a rate of 10 °C/min from 50 to 800 °C.

4.2.2. Fourier transform infrared spectrometry (FT-IR)

Fourier transform infrared spectrometry (FT-IR) has been used to identify interactions in polymer blends. For the FT-IR analysis, a mixture of catalyst samples with IR-grade KBr was shaped into a pellet and pressed into a disk in a vacuum box. The FT-IR spectra were obtained using a Nicolet 6700 spectrometer with 150 scans and a resolution of 2 cm⁻¹ in the range of 400 to 4000 cm⁻¹.

4.2.3. Thermogravimetric analysis (TGA)

Thermogravimetric analysis (TGA) was performed using an SDT Q600 to measure the amount of carbons deposited by the SCR reaction. We used 65–125 mg of catalysts and an air flow rate of 100 mL/min for the TGA. The temperature for TGA

experiments was increased from ambient temperature to 800°C at a rate of 10°C/min.

4.3 XRD analysis

XRD analysis of the $\text{La}_{0.8}\text{Sr}_{0.2}\text{NiO}_3$ perovskite-type catalyst was performed to investigate the structural properties at different PVP molarities (0.5–5.0 M), as shown in Fig. 24. The main characteristic peaks of a perovskite structure at 1 M PVP appeared at $2\theta = 23^\circ, 33^\circ, 47^\circ, 58^\circ$, and 68° (JCPDF No.33-0710) without additional peaks. However, at PVP molarities other than 1 M, SrCO_3 peaks were observed at $2\theta = 32^\circ, 43^\circ$, and 55° (JCPDF No.05-0418), and when 5 M PVP was used, a NiO peak appeared at 62° (JCPDS No.44-1159). This means that at 1 M PVP, the perovskite structure was obtained exclusively as only perovskite peaks could be observed (in contrast to the other concentrations). The peak intensity of SrCO_3 increased as the PVP molarity was either increased or decreased from 1 M. At the optimal concentration of 1 M, metal oxide particles did not agglomerate, preventing other crystal structures from forming.

The particle sizes of SrCO_3 are presented in Table 6, and the mean size was calculated using the Scherrer equation shown in Eq. 10

$$\tau = \frac{K\lambda}{\beta \cos\theta} \quad (10)$$

where τ is the mean size of the ordered (crystalline) domains, which may be smaller or equal to the grain size. K is the dimensionless shape factor, which typically has a value of 0.9. The λ and β factors are the X-ray wavelength and line broadening at half the maximum intensity (FWHM), respectively. Corresponding to the trend in peak intensity, the SrCO_3 particles increased in size when the PVP molarity was either higher or lower than 1 M. The size increases because degradation of the perovskite crystal structure allows Sr to be easily carbonated during agglomeration. In general, Sr was partially substituted for La site in the perovskite structure to improve the lattice

oxygen mobility which plays a role in the reforming reaction and coke removal. At PVP molarities other than 1 M, the Sr was significantly carbonated (SrCO_3), which decreased the lattice oxygen mobility that affects the reactivity.

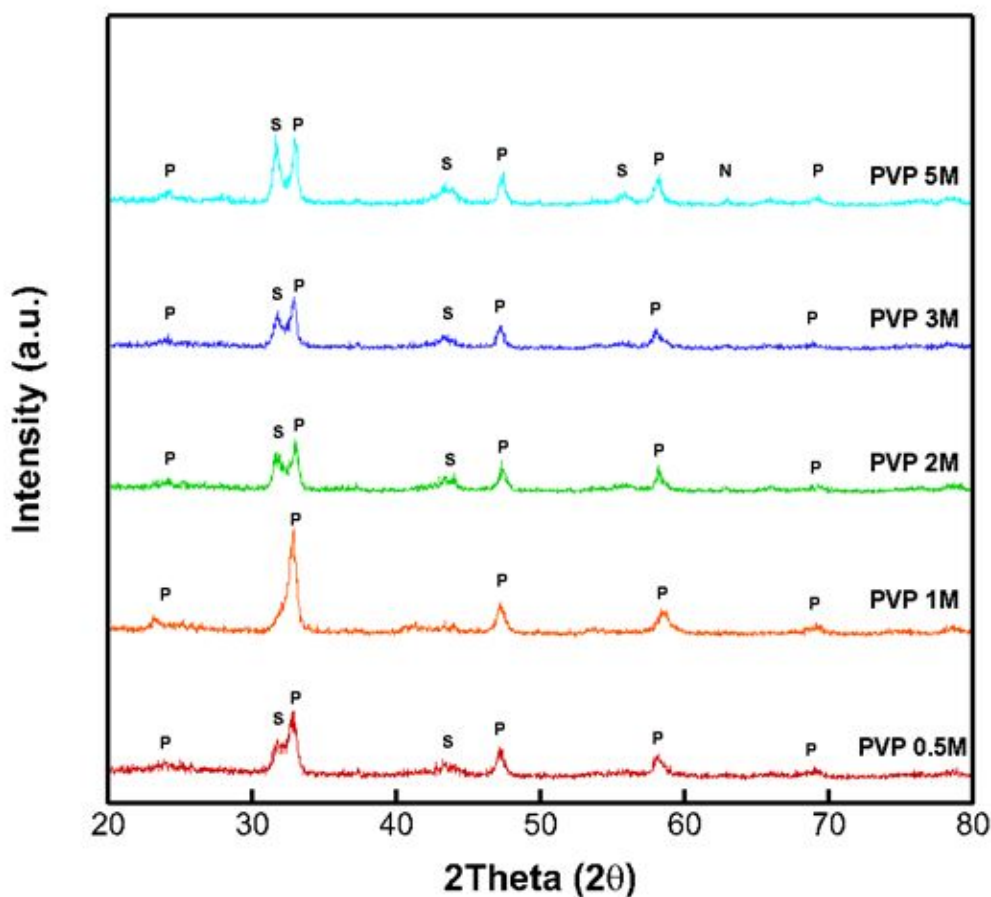


Fig. 24. XRD patterns of $\text{La}_{0.8}\text{Sr}_{0.2}\text{NiO}_3$ perovskite-type catalysts at different PVP molarities: (P) perovskite, (S) SrCO_3 , and (N) NiO .

Table 6. SrCO_3 particle sizes at different PVP molarities

	PVP molarity (M)				
	0.5	1	2	3	5
SrCO_3 particle size (nm)	1.51	-	1.20	2.02	2.02

4.4 H₂-TPR profiles

Fig. 25 shows the H₂-TPR profiles used to characterize the reducibility of perovskite-type catalysts at different PVP molarities. The two main transition peaks were exhibited within the temperature regions of 300–400°C and 450–600°C. The transition peak at 300–400°C can be assigned to the reduction of Ni³⁺ to Ni²⁺, whereas the transition peak at 450–600°C corresponds to the reduction of Ni²⁺ to Ni⁰. However, the catalyst reducibility at the site of Ni²⁺ significantly varies with respect to PVP molarity. The reduction temperature was highest at 522°C (H₂ consumption) when 1 M PVP was used to prepare the catalyst. However, the transition peak was shifted towards a lower reduction temperature at higher PVP molarities. The difference in the reduction temperature for catalysts prepared with 1 M and 5 M PVP was 27°C.

In general, the perovskite-type catalyst prepared with 5 M PVP would have a higher reducibility, but it would be at the expense of weakening the interactions between catalyst particles. The consequence of weakened interactions is deactivation of the catalyst by the sintering of metal particles at high temperature. On the other hand, the perovskite-type catalyst prepared with 1 M PVP would have superior stability because of strong interactions between metallic catalyst particles.

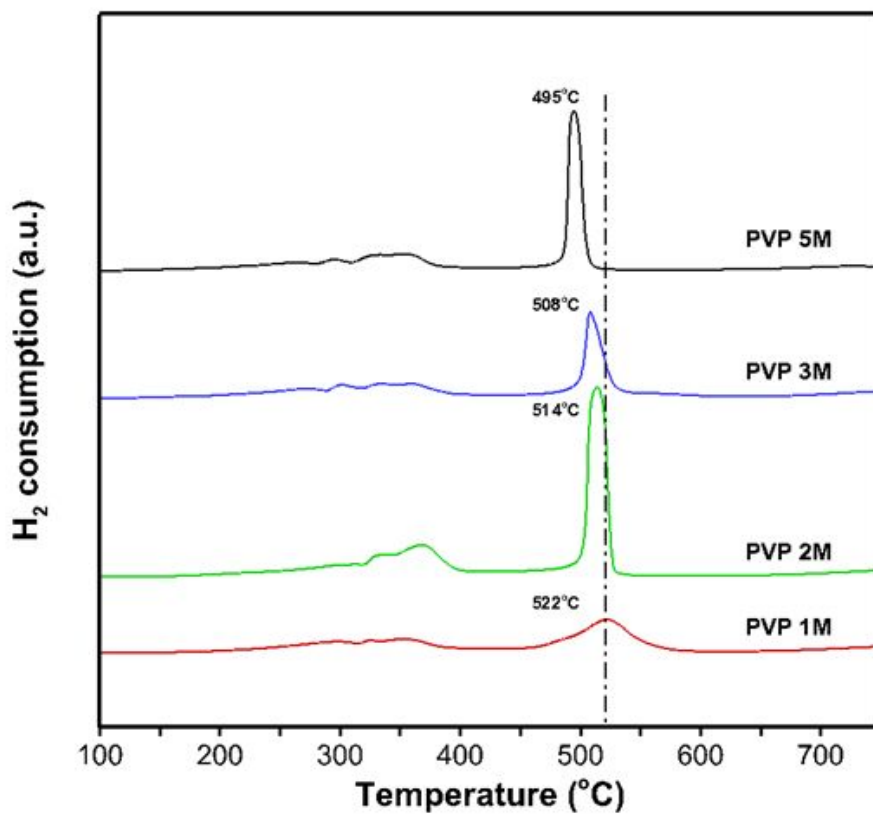


Fig. 25. TPR profiles of $\text{La}_{0.8}\text{Sr}_{0.2}\text{NiO}_3$ perovskite-type catalysts at different PVP molarities.

4.5 FT-IR analysis

The FT-IR adsorption spectra of the perovskite-type catalyst at different PVP molarities are shown in Fig. 26. Absorption bands at 856 cm^{-1} and 1450 cm^{-1} were observed in all spectra. The absorption band at $\sim 665\text{ cm}^{-1}$ is characteristic of the stretching vibration of hydroxyl groups that are hydrogen bonded to Ni–O. In general, the free planar CO_3^{2-} complexes have D_{3h} symmetry, and their vibrations correspond to absorption bands at $400\text{--}1800\text{ cm}^{-1}$. The strong absorption band centered at $\sim 1450\text{ cm}^{-1}$ denotes the asymmetric stretching vibrations of SrCO_3 . The absorption band of SrCO_3 at 856 cm^{-1} can be assigned to out-of-plane bending vibrations. No carbonate phase was observed in the XRD pattern of the catalyst prepared with 1 M PVP because only long-range ordered materials can be identified by the XRD technique. However, it was revealed by FT-IR analysis that highly dispersed carbonate crystallites exist on the perovskite-type catalyst.

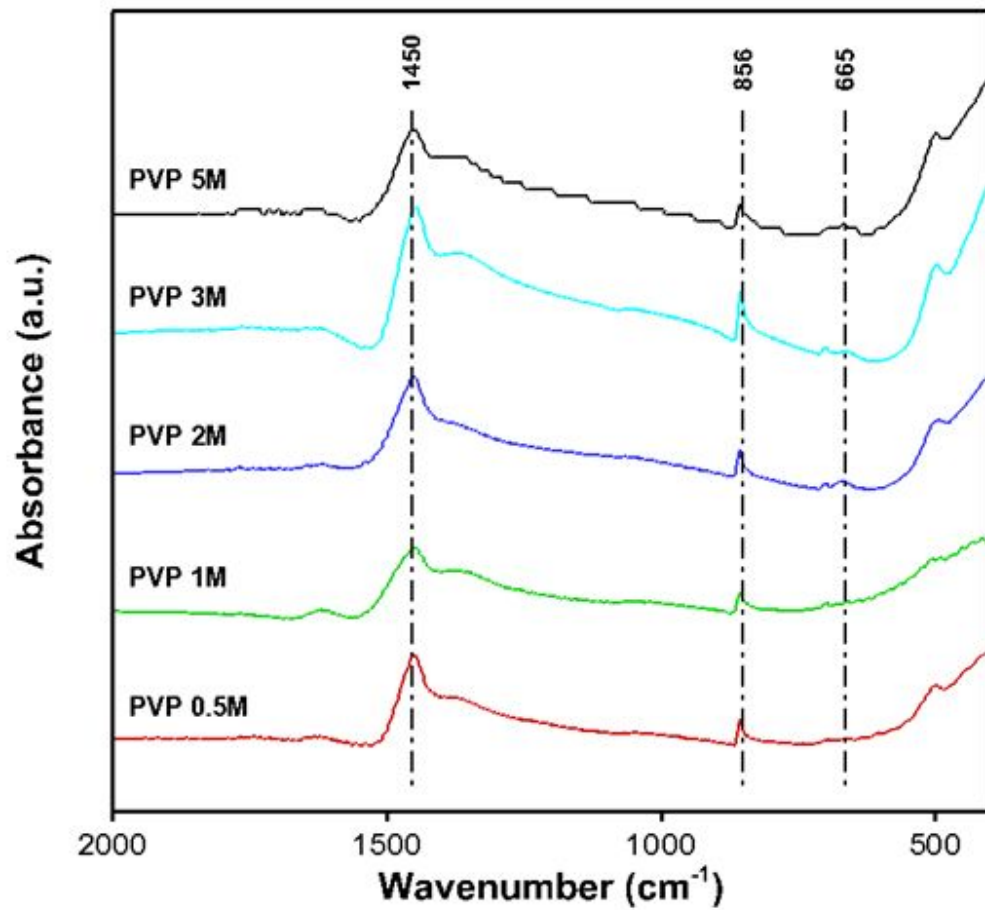


Fig. 26. FT-IR adsorption spectra of the perovskite-type catalysts at different PVP molarities.

4.6 Reactivity of reforming

Conversions of CH_4 and CO_2 using the perovskite-type catalyst as a function of PVP molarity for the SCR and DR reaction are shown in Fig. 27. Maximal CH_4 and CO_2 conversions were achieved when 1 M PVP was used, and the conversions decreased with increasing PVP molarity from 1 to 5 M. The dependency of conversion on PVP molarity was quite significant; the CH_4 conversion was 73.3% at 1 M PVP and 24.7% at 5 M PVP, and the CO_2 conversion was 46.9% at 1 M PVP and 12.1% at 5 M PVP for the SCR reaction, as shown in Fig. 27 (a). Also, conversions of CH_4 and CO_2 using the perovskite-type catalyst as a function of PVP molarity for the DR reaction, as shown in Fig. 27 (b). As a result, maximal CH_4 and CO_2 conversions were achieved when 1 M PVP was used, and the conversions decreased with increasing PVP molarity from 1 to 3 M. The dependency of conversion on PVP molarity was quite significant; the CH_4 conversion was 87.7% at 1 M PVP and 80.2% at 0.5 M PVP, and the CO_2 conversion was 92.1% at 1 M PVP and 87.0% at 0.5 M PVP. This dependency is linked to the increasing sizes of SrCO_3 particles when the PVP molarity is increased, as shown in the XRD pattern (Fig. 24) and Table 6. Larger SrCO_3 particles cause a low dispersion of perovskite-type catalysts, which results in the diminished catalytic activity depicted in Fig. 27.

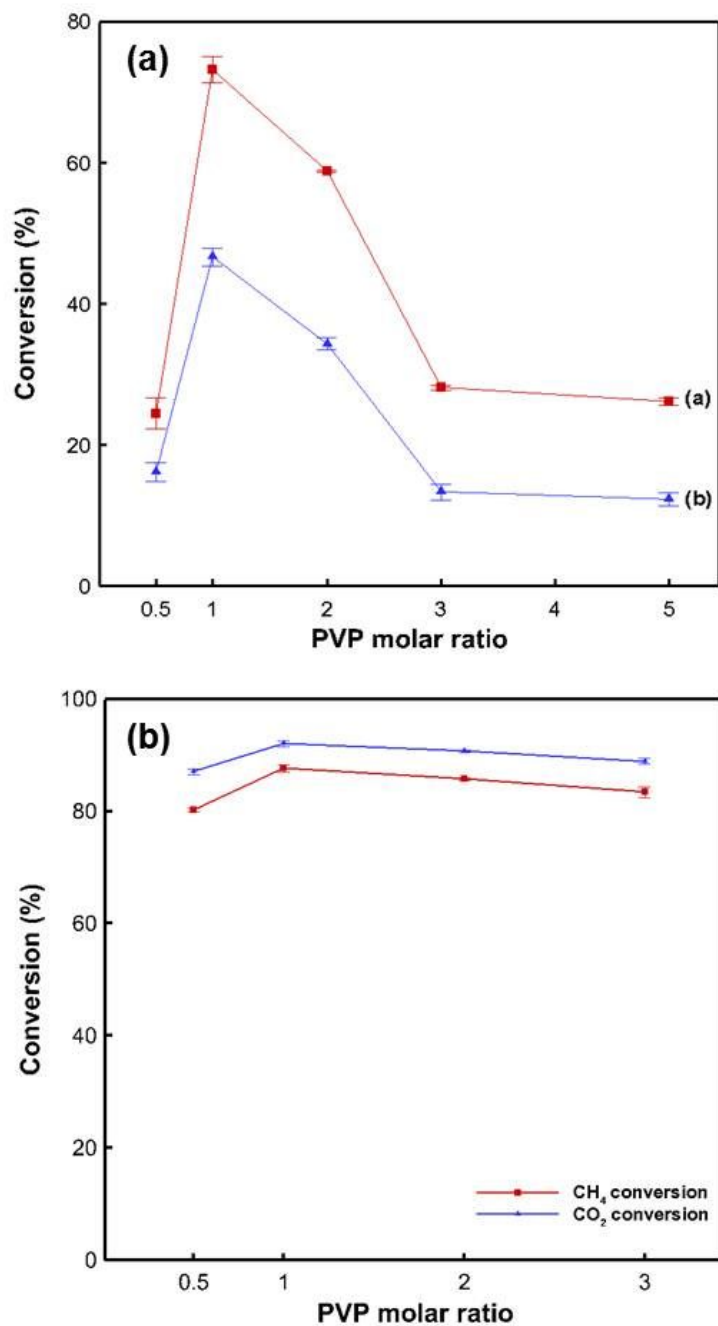


Fig. 27. Reactivity of the perovskite-type catalysts at different PVP molarities: (a) SCR of methane and (b) DR of methane, (■) CH₄ conversion and (▲) CO₂ conversion.

4.7 Carbon deposition (TGA)

Carbon deposition can deactivate catalysts during reforming reactions. Carbon can be deposited via the Boudouard reaction, CH₄ decomposition, CO₂ hydrogenation, and CO hydrogenation. The use of perovskite-type catalysts in place of Ni catalysts for reforming reactions can suppress carbon formation. The amount of carbons deposited onto the perovskite-type catalysts during the SCR reaction was measured by TGA analysis. The Ni catalyst was also reacted under the same reaction conditions for comparison with perovskite-type catalysts. The profiles of weight loss are shown in Fig. 28.

The TGA oxidation curve of perovskite-type catalysts exhibited two following transitions: a slight increase in weight due to the oxidation of active metal sites and a decrease attributed mainly to the decomposition of the La₂O₂CO₃ phase. The activated CO₂ was preferentially adsorbed on the La₂O₃ support to form a carbonate phase, as expressed in Eq. 11 [55-56].



The carbon deposition of SCR was 0.3–0.4% on the perovskite-type catalyst, whereas it was 1.9% on the Ni catalyst. And, the carbon deposition DR was 0.4-0.6% on the perovskite-type catalyst, whereas it was 6.2% on the Ni catalyst, which indicates that the perovskite-type catalyst can better suppress carbon deposition.

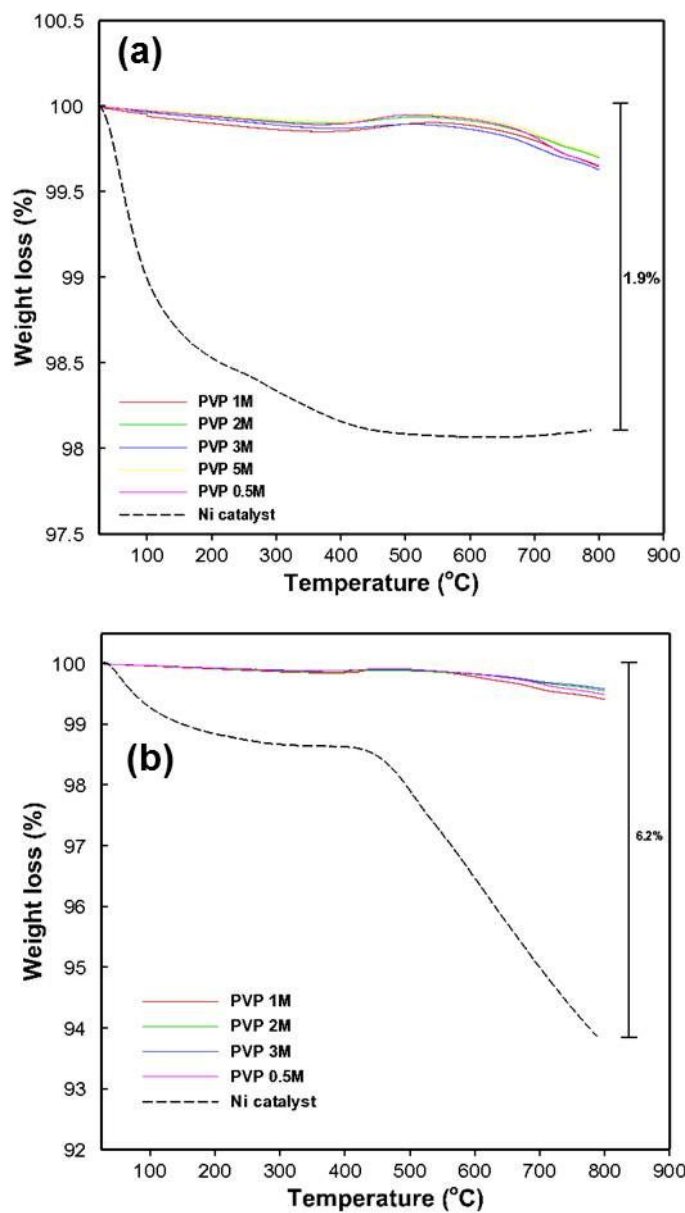


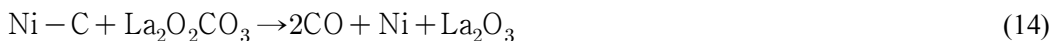
Fig. 28. TGA analysis of perovskite-type catalysts and Ni catalyst after reacting for 12 h: (a) SCR of methane and (b) DR of methane.

4.8 Surface reaction mechanism

Fig. 29 shows a schematic diagram presenting the proposed reaction mechanism on the reduced perovskite-type catalyst with and without the addition of water. The catalyst is reacted with CH_4 , CO_2 , and H_2O after being reduced by H_2 . CH_4 is absorbed on the Ni active site and dissociates to slowly form 2 moles of hydrogen and a Ni-C species as the adsorbed state (Eq. 12). Meanwhile, CO_2 is adsorbed on the La_2O_3 support and a $\text{La}_2\text{O}_2\text{CO}_3$ carbonate layer forms quickly (Eq. 13)



At high temperature, $\text{La}_2\text{O}_2\text{CO}_3$ subsequently reacts with surface carbon species on Ni active sites (Ni-C) to produce CO, restoring the Ni metal particles and La_2O_3 (Eq. 14). La_2O_3 functions as a promoter and as an intermediate to react the carbon species with CO_2 , as shown in Fig. 29 (a). Because of the role La_2O_3 plays in this process, carbon deposition would occur less frequently on the perovskite-type catalyst than on the Ni catalyst.



When water is added, Ni-C reacts with water to form H_2 and CO (coke gasification, Eq.15; shown in Fig. 29 (b)).



These mechanisms aptly detail why carbon deposition is reduced on perovskite-type catalysts during the SCR reaction. The XRD patterns obtained after the reaction are

shown in Fig. 30. Most of the peaks could be assigned to $\text{La}_2\text{O}_2\text{CO}_3$ (JCPDF No. 37-0804), whereas only traces of SrCO_3 , La_2O_3 (JCPDF No. 22-0369), and La_2NiO_4 (JCPDF No.34-0347) were observed. This agrees well with the formations described in Eq. 13 and 14. SEM images of the catalyst surfaces before and after the reaction are shown in Fig. 31, and the morphologies were observably different. The fresh catalyst showed small particles (Fig. 31 (a)), but after the reaction, larger particles were observed (Fig. 31 (b)). Based on the SEM images and XRD results, we estimate that the large particles formed by the reaction correspond to $\text{La}_2\text{O}_2\text{CO}_3$ and that the other small particles were SrCO_3 , La_2O_3 , and La_2NiO_4 .

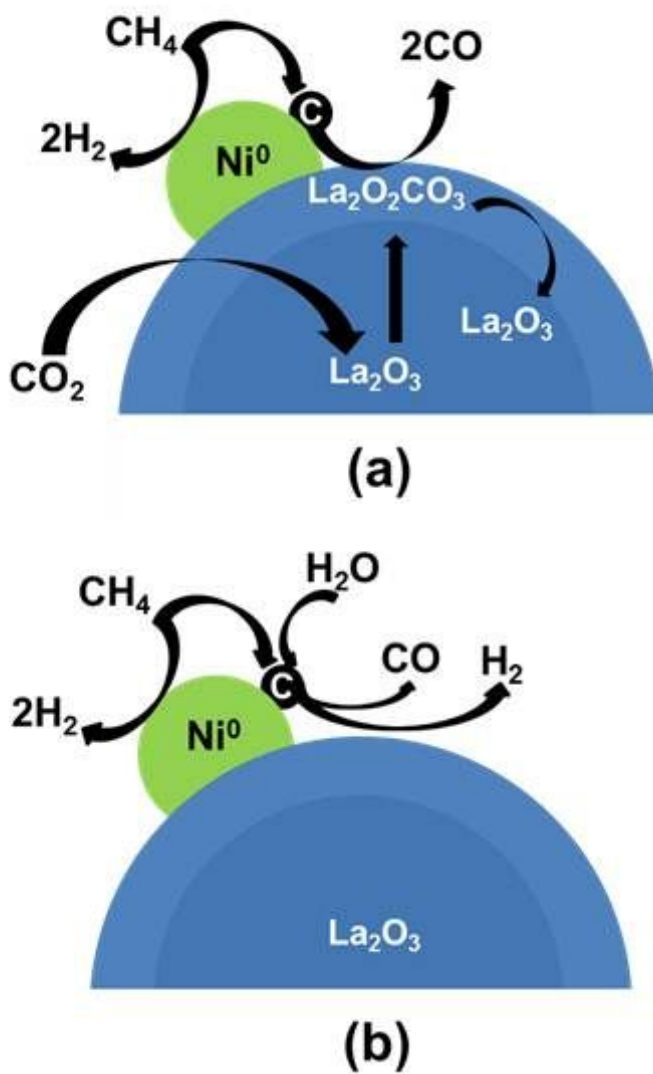


Fig. 29. Proposed surface mechanism over the reduced perovskite-type catalyst: (a) reaction of the carbon species with CO_2 and (b) coke gasification with the addition of water.

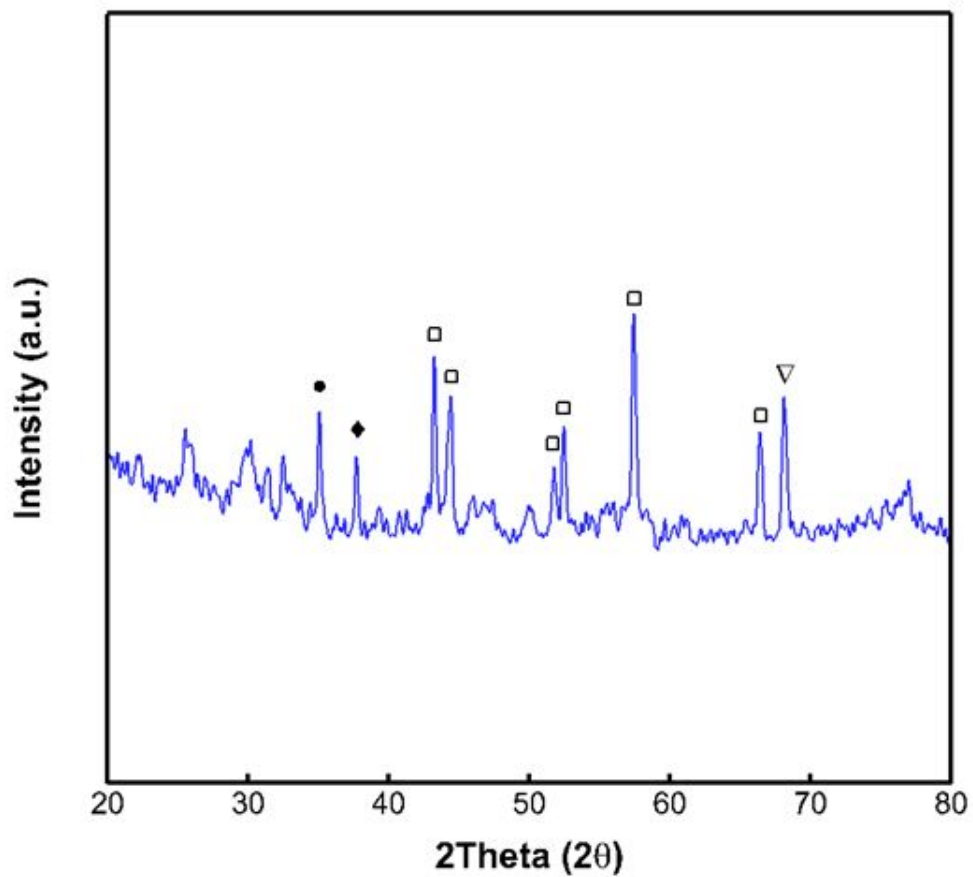


Fig. 30. XRD patterns of the perovskite-type catalysts after the reaction: (●) La_2NiO_4 , (◊) $\text{La}_2\text{O}_2\text{CO}_3$, (□) La_2O_3 , and (▽) SrCO_3 .

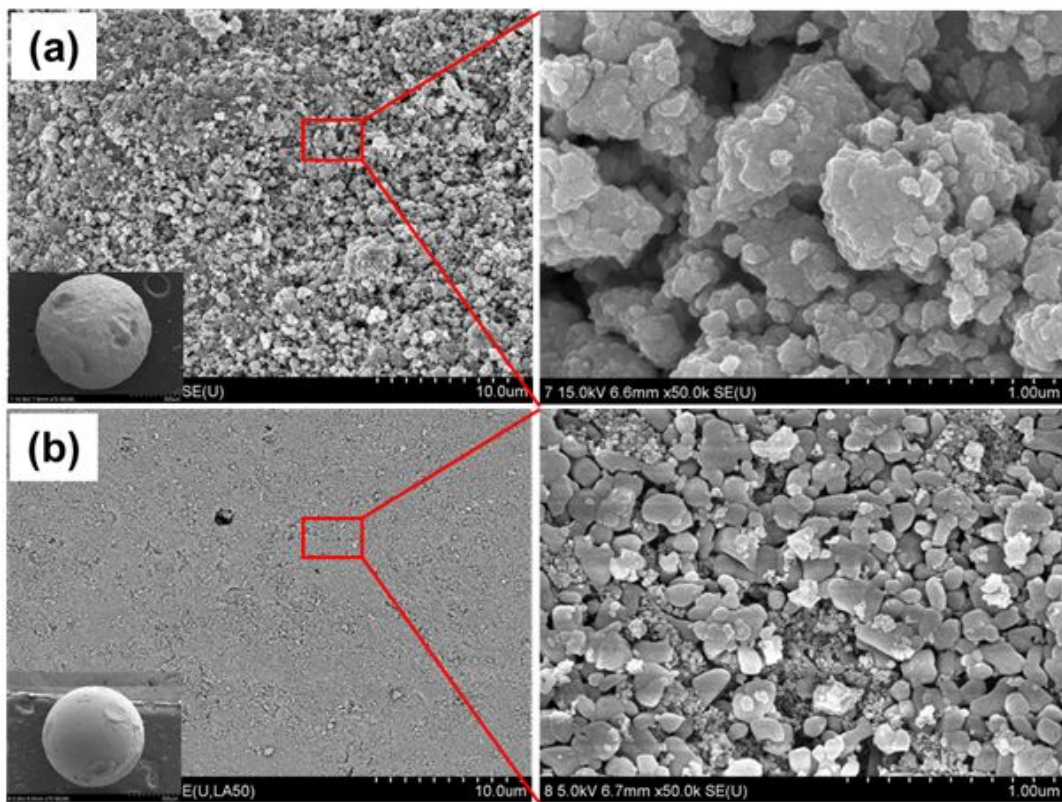


Fig. 31. SEM images of the perovskite-type catalysts: (a) before the reaction and (b) after the reaction.

Chapter 5. Perovskite-type catalysts (Other sol-gel method)

5.1. Preparation of perovskite type catalyst

The perovskite type catalysts, $\text{La}_{0.8}\text{Sr}_{0.2}\text{NiO}_3$ were prepared by sol-gel method and EDTA cellulose method. PVA (Alfa Aesar Co.), PAA (Sigma- Aldrich) and EDTA (Samchun pure chemical Co.) were dissolved in distilled water that is heated at 65°C for 30 min, respectively. After that, $\text{La}(\text{NO}_3)_3$ (Samchun pure chemical Co.), $\text{Sr}(\text{NO}_3)_2$ (Samchun pure chemical Co.) and $\text{Ni}(\text{NO}_3)_2$ (Samchun pure chemical Co.) dissolved in PVA, PAA and EDTA solution, respectively. However, the pH of the EDTA solution was controlled by adding NH_4OH (Samchun pure chemical Co.) and its pH was maintained at 9.0. After three solutions were evaporated at a hot plate with 80°C for 30 min, the perovskite sol was obtained. It followed that the sol was dried at a convection oven with 100°C for 12 hr and was pre-calcined at 800°C ($2.5^\circ\text{C}/\text{min}$) for 5 hr. Consequently, the perovskite type catalyst, $\text{La}_{0.8}\text{Sr}_{0.2}\text{NiO}_3$ was obtained as a fine powder.

5.2. Characterization and Reaction Test

The perovskite type catalysts were analyzed by X-ray diffraction (XRD, D/MAX-3C), H₂-Thermal programmed reduction (H₂-TPR, Chemisorption Analyzer BEL-CAT) and Fourier transform infrared spectroscopy (FT-IR, Nicolet 6700)

Fig. 32 shows and experimental setup for the SCR and DR reaction on the La_{0.8}Sr_{0.2}NiO₃/γ-Al₂O₃. A fixed bed reactor was used in which the perovskite catalyst was packed. An Inconel tube with 0.92 cm in diameter and 40 cm in length was used as a reactor. The loading of the catalysts were 1.45 g (SCR) and 0.74 g (DR). The reaction temperature and GHSV were fixed to 800°C and 20,000h⁻¹ at the all reactions. Before the reaction, the perovskite catalyst was reduced in a hydrogen condition at 800°C with a feed rate of 50 mL/min for 2 hr. The feed ratio of CH₄: H₂O: CO₂ as reactants was fixed to 1.0: 2.0: 1.0 and 1.0: 0: 1.0 for SCR and DR reaction, respectively. The reactants were mixed and heated up to 300°C through a pre-heater and supplied for the SCR and DR reactions. The gaseous products were analyzed by GC equipped with a TCD and FID.

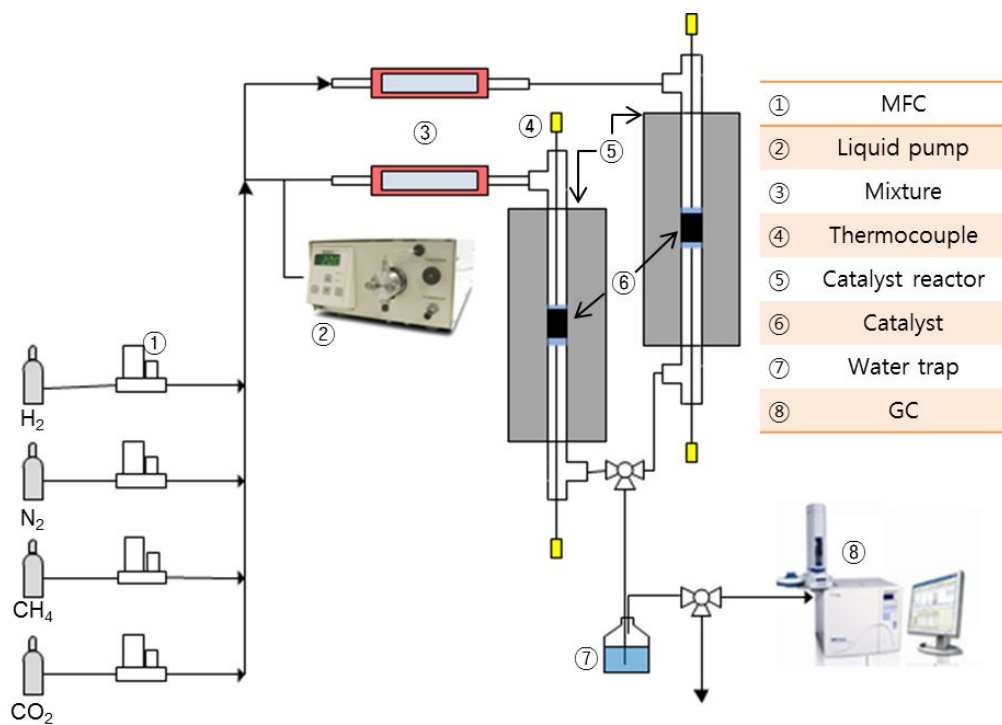


Fig. 32. Experimental setup for SCR and DR of methane reaction.

5.3. Catalyst characterization

Fig. 33 shows the XRD patterns of all perovskite type catalyst. The perovskite, NiO and SrCO_3 peaks were detected. The $\text{La}_{0.8}\text{Sr}_{0.2}\text{NiO}_3$ exhibited the main characteristic peaks of perovskite type structure at $2\theta=23^\circ, 33^\circ, 47^\circ, 58^\circ$ and 68° with the absence of additional peaks. However, the NiO peaks at 31° and 42° , and SrCO_3 peak at 43° were only detected at PAA and EDTA agents. It means that PVA agent established more definite perovskite structures during the gelation than other agents.

Infrared spectroscopy has been used to identify interactions in the blend of polymers. FT-IR is very sensitive to the formation of hydrogen bonds. Fig. 34 shows the FT-IR absorption spectra of all perovskite type catalyst in the wavenumber range of 800-4000 cm^{-1} .

For all perovskite type catalyst, the band at 1310 cm^{-1} was assigned to CH_2 out of plane bending. The band at 2490 cm^{-1} corresponded to secondary amide ($-\text{NH}$). The band at 2870 cm^{-1} corresponded to C-H bending. The three band absorption peak of PVA agent catalyst were higher than that of PAA and EDTA agent catalysts. In general, the intensity of FT-IR absorption implies the amplitude of dipole moment in the molecule. The polarity of chemical bonds can be identified from the dipole moment. The increase of the dipole moment means the increase of the polarity across the chemical bond, resulting in the increase of molecule movements. It means that molecules got more active to the reaction. The PVA agent catalyst had the highest absorbance of CH_2 , $-\text{NH}$, and C-H bending compared to PAA and EDTA agent catalyst. Therefore, the activity of PVA agent catalyst would be increased.

Fig. 35 shows the H_2 -TPR profiles characterizing the reducibility of all perovskite type catalysts. The perovskite exhibited two main transition peaks at temperature ranges of $300\text{-}400^\circ\text{C}$ and $450\text{-}600^\circ\text{C}$. The $300\text{-}400^\circ\text{C}$ transition peak was assigned to the reduction of Ni^{3+} to Ni^{2+} . The $450\text{-}600^\circ\text{C}$ transition peak was assigned to the reduction of Ni^{2+} to Ni^0 .

However, it was found that the reducibility of these catalysts was significantly changed at the two sites of the perovskite type catalyst according to the gelation agents. The two transition peaks of PVA agent catalyst shifted into lower reduction

temperature so it indicated its higher reducibility. In general, smaller particle sizes of nickel with its high reducibility are responsible for enhancing the transport of reactants, resulting that the catalytic activity was improved.

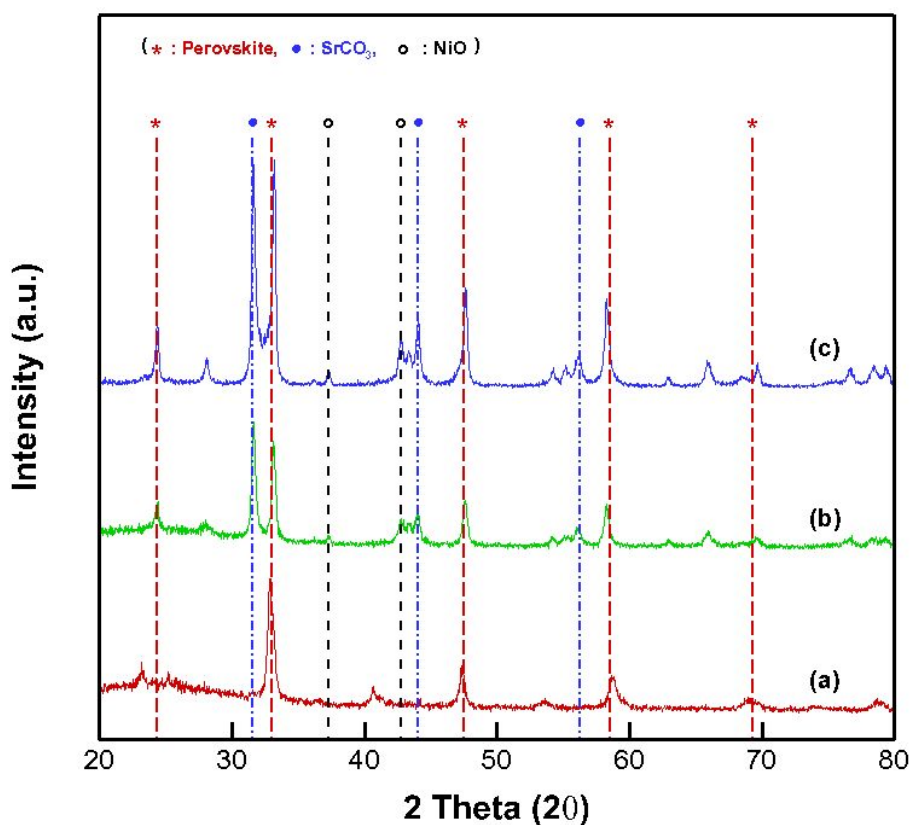


Fig. 33. XRD patterns of the perovskite type catalysts according to the gelation agents; (a) PVA, (b) PAA and (c) EDTA agent.

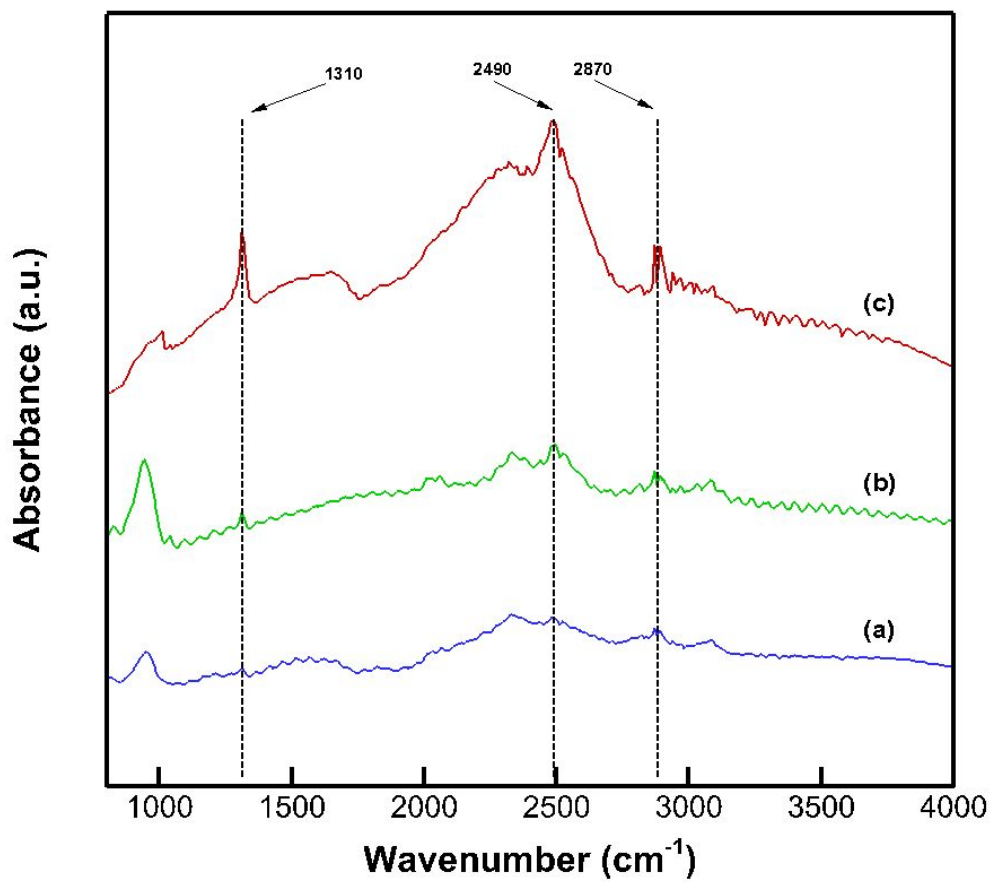


Fig. 34. FT-IR of the perovskite type catalysts according to the gelation agents; (a) EDTA, (b) PAA and (c) PVA agent.

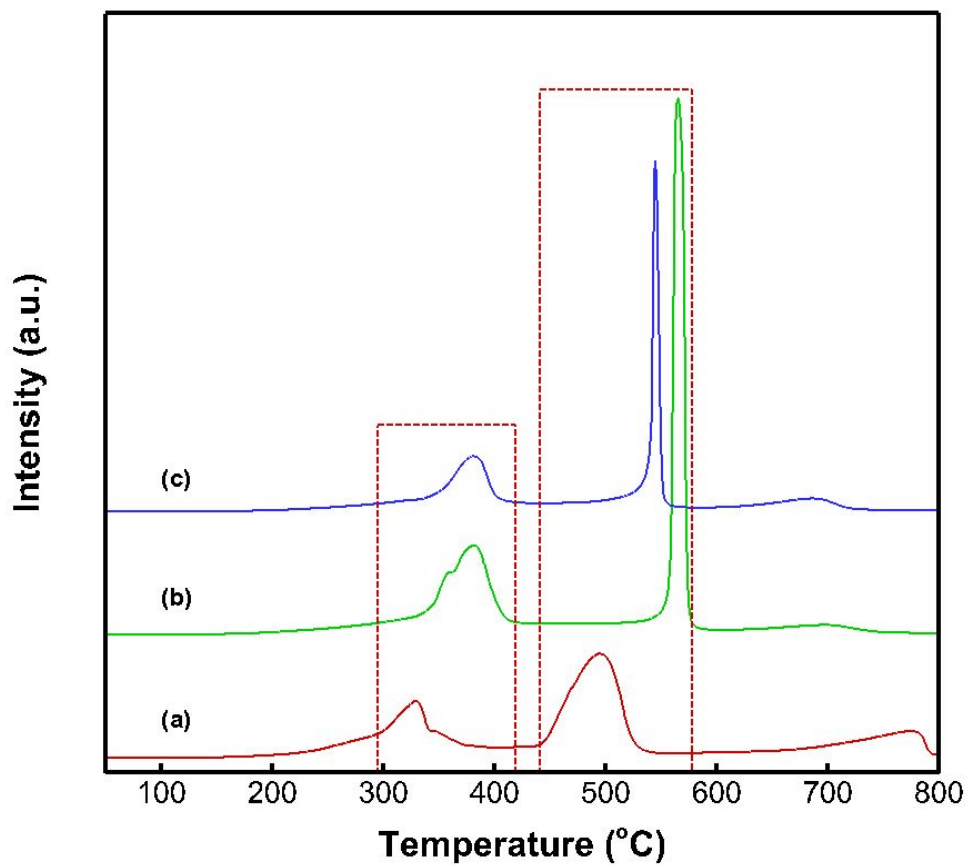


Fig. 35. H₂-TPR profiles of the perovskite-type catalyst according to the gelation agents; (a) PVA, (b) PAA and, (c) EDTA agent.

5.3. Effect of gelation agents on the reactivity of perovskite type catalyst

Fig. 36 shows the CH_4 and CO_2 conversions of perovskite type catalysts for SCR and DR reaction. The CH_4 and CO_2 conversions of the PVA agent catalyst were much higher than that of the PAA and EDTA agent catalyst for DR reaction as shown in Fig. 36 (a). This result agreed with results of XRD, FT-IR and H_2 -TPR showing that the PVA agent catalyst had a strong perovskite structure, a high absorption and a high reducibility. For SCR reaction, However, the CH_4 and CO_2 conversions of the PAA agent catalyst was higher than that of the PVA and EDTA agent catalyst as shown in Fig. 36 (b). It means that the addition of water affected the perovskite catalyst during the reaction. Generally, the water tends to make it weaker that the interaction of catalysts. Based on the H_2 -TPR result, the PAA agent catalysts due to a high reduction temperature. That is why the PAA agent catalyst showed high conversions for the SCR reaction.

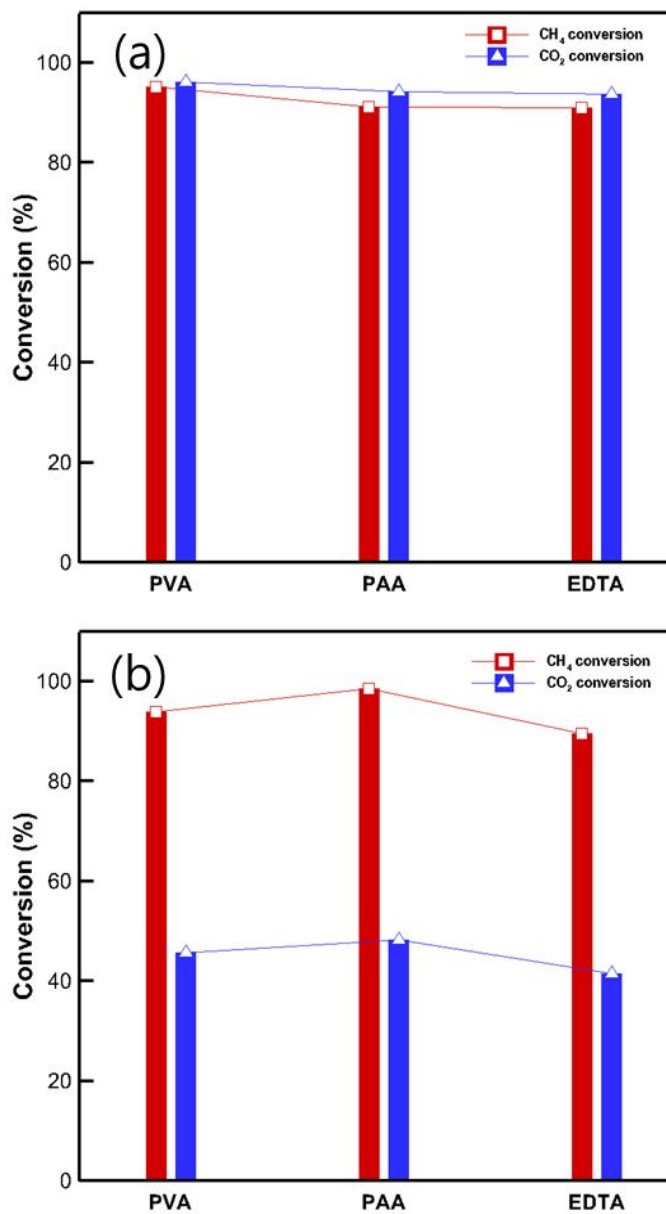


Fig. 36. CH_4 and CO_2 conversions of the perovskite-type catalysts according to the gelation agents at different reactions; (a) DR of methane and (b) SCR of methane.

Chapter 5. Conclusion

A catalyst supported on the Ni foam was developed to improve the mass and heat transfer through the SCR reactor for GTL-FPSO applications. The metallic foam catalyst was composed of Ni active sites, a γ - Al_2O_3 supporting layer, and a Ni foam substrate. The Ni/ γ - Al_2O_3 /Ni foam catalyst was characterized and evaluated under a range of conditions, such as temperature and space velocity. The uniform catalyst layer was formed on the surface of the Ni foam. The catalyst dispersion was reduced as the calcination temperature was increased because the particle size of NiO increased with increasing calcination temperature. The thermal dispersion of the metallic foam catalyst during the reaction was better than that of the pellet catalyst because the metallic foam catalyst had a uniform temperature distribution through out the SCR reactor. The CH_4 and CO_2 conversions increased with increasing temperature. The syngas production rate also increased with increasing temperature, where as the molar ratio of syngas decreased. The metallic foam catalyst had high conversions of CH_4 and CO_2 at a high space velocity. The durability of the catalyst was evaluated by a long-term reaction at a high space velocity for 50 hours. The CH_4 and CO_2 conversions decreased by 10% compared to that after the reaction was initiated. The catalyst degradation was caused by carbon deposition and crack formation on the catalyst surface.

Also, The optimal composition of the wash-coating sol was determined. When the Al_2O_3 /AIP molar ratio was 5, surface cracks were not observed and the weight fraction of the Al_2O_3 wash-coat layer on the Ni foam was 20 wt.% when wash-coated 5 times. The fall-off test revealed the highest adhesion at an Al_2O_3 /AIP molar ratio of 5. As a result of the heat transfer characteristics, the radial heat transfer of the metallic foam catalyst was improved. The Nusselt number of the metallic foam catalyst was higher than that of the conventional pellet catalyst, and the difference between both catalysts increased with increasing space velocity. Consequently, the metallic foam catalyst can maintain a uniform temperature distribution through the reactor with a high space velocity (either an increased gas feed rate or decreased reactor size). Therefore, the metallic foam catalyst is more suitable for GTL-FPSO applications in terms of the

reformer compactness and the mechanical strength of the catalyst.

In chapter 4, a perovskite-type catalyst was developed to prevent carbon deposition during the SCR reaction for the GTL-FPSO process. Specifically, we successfully prepared a $\text{La}_{0.8}\text{Sr}_{0.2}\text{NiO}_3$ perovskite catalyst supported on $\alpha\text{-Al}_2\text{O}_3$ using a polyol method. The catalyst was characterized and evaluated for a range of employed PVP molarities during preparation. At 1 M PVP, the characteristic peaks of a perovskite structure were predominantly expressed, whereas peaks corresponding to SrCO_3 and NiO became observable at other molarities of PVP. The catalyst prepared with 1 M PVP was also more stable due to the strong interactions between metal particles. Therefore, an ideal PVP concentration allowed us to optimize the SCR reactivity on the perovskite catalyst by allowing us to restrict the size of SrCO_3 particles. The carbon deposition was 0.3–0.4% on the perovskite-type catalyst and 1.9% on the Ni catalyst. Therefore, the $\text{La}_{0.8}\text{Sr}_{0.2}\text{NiO}_3$ perovskite catalyst demonstrated a superior ability to prevent carbon deposition.

Reference

1. D. Schanke, P. Lian, S. Eri, E. Rytter, B.H. Sanns, K.J. Kinnari, Optimization of Fischer–Tropsch reactor design and operation in GTL plant, *Stud. Surf. Sci. Catal.* 136 (2001) 239–244.
2. R. Khalilpour, I.A. Karimi, Evaluation of utilization alternatives for stranded natural gas, *Energy* 40 (2012) 317–328.
3. F. Yagi, R. Kanai, S. Wakamatsu, R. Kajiyama, Y. Suehiro, M. Shimura, Development of synthesis gas production catalyst and process, *Catal. Today* 104 (2005) 2–6.
4. W.F.J. Burgers, P.S. Northrop, H.S. Khesghi, J.A. Valencia, Worldwide development potential for sour gas, *Energy Procedia* 4 (2011) 2178–2184.
5. J. T Richardson, M. Garrait, J.K Hung, Carbon dioxide reforming with Rh and Pt-Re catalysts dispersed on ceramic foam supports, *Appl. Catal. A: Gen.* 225 (2003) 69–82.
6. N. Gokon, Y. Osawa, D. Nakazawa, T. Kodama, Kinetics of CO₂ reforming of methane by catalytically activated metallic foam absorber for solarr eceiver-reactors, *Int. J. Hydrogen Energy* 34 (2009) 1787–1800.
7. L. Giani, C. Cristiani, G. Groppi, E. Tronconi, Washcoating method for Pd/γ-Al₂O₃ deposition on metallic foams, *Appl. Catal. B: Environ.* 62 (2006) 121–131.
8. K. Sutthiumporn, T. Maneerung, Y. Kathiraser, S. Kawi, CO₂ dry-reforming of methane over La_{0.8}Sr_{0.2}Ni_{0.8}M_{0.2}O₃ perovskite (M=Bi, Co, Cr, Cu, Fe); Roles of lattice oxygen on C-H activation and carbon suppression, *Int. J. Hydrogen Energy* 37 (2012) 11195–11207.
9. M.K. Nikoo, N.A.S. Amin, Thermodynamic analysis of carbon dioxide reforming of methane in view of solid carbon formation, *Fuel Process. Technol.* 92 (2011) 678–691.
10. J.T. Richardson, Y. Peng, D. Remue, Properties of ceramic foam catalyst supports; pressure drop, *Appl. Catal. A: Gen.* 204 (2000) 19–32.
11. L. Giani, G. Groppi, E. Tronconi, Mass-transfer characterization of metallic foams

- as supports for structured catalysts, *Ind. Eng. Chem. Res.* 44 (2005) 4993-5002.
12. R.D. Gonzalez, T. Lopez, R. Gomez, Sol-Gel preparation of supported metal catalysts, *Catal. Today* 35 (1997) 293-317.
 13. M. Valentini, G. Groppi, C. Cristiani, M. Levi, E. Tronconi, P. Forzatti, The deposition of γ -Al₂O₃ layers on ceramic and metallic supports for the preparation of structured catalysts, *Catal. Today* 69 (2001) 307-314.
 14. H. Schulz, Short history and present trends of Fischer-Tropsch synthesis, *Appl. Catal. A: Gen.* 186 (1999) 3-12.
 15. J.A. Velasco, L. Lopez, M. Velásquez, M. Boutonnet, S. Cabrera, S. Järås, Gas to liquids: A technology for natural gas industrialization in Bolivia, *J. Nat. Gas. Sci. Eng.* 2 (2010) 222-228.
 16. G. Bian, T. Nanba, N. Koizumi, M. Yamada, Changes in microstructure of a reduced cobalt catalyst during performing FT synthesis from syngas determined by in situ high-pressure syngas adsorption, *J. Mol. Catal. A: Chem.* 178 (2002) 219-228.
 17. B.T. Schädel, M. Duisberg, O. Deutschmann, Steam reforming of methane, ethane, propane, butane, and natural gas over a rhodium-based catalyst, *Catal. Today* 142 (2009) 42-51.
 18. T. Namioka, A. Saito, Y. Inoue, Y. Park, T-J. Min, S-A. Roh, K. Yoshikawa, Hydrogen-rich gas production from waste plastics by pyrolysis and low-temperature steam reforming over a ruthenium catalyst, *Appl. Energ.* 88 (2011) 2019-2026.
 19. A. Nandini, K.K. Pant, S.C. Dhingra, Kinetic study of the catalytic carbon dioxide reforming of methane to synthesis gas over Ni-K/CeO₂-Al₂O₃ catalyst, *Appl. Catal. A: Gen.* 380 (2006) 119-127.
 20. A.M. Ghorbanzadeh, R. Lotfalipour, S. Rezaei, Carbon dioxide reforming of methane at near room temperature in low energy pulsed plasma, *Int. J. Hydrogen Energy* 34 (2009) 293-288.
 21. X.X. Gao, C.J. Huang, N.W. Zhang, J.H. Li, W.Z. Weng, H.L. Wan, Partial oxidation of methane to synthesis gas over Co/Ca/Al₂O₃ catalysts, *Catal. Today* 131 (2008) 211-218.

22. P. Kim, Y. Kim, H. Kim, I.K. Song, J. Yi, Synthesis and characterization of mesoporous alumina with nickel incorporated for use in the partial oxidation of methane into synthesis gas, *Appl. Catal. A: Gen.* 272 (2004) 157-166.
23. T. Takeguchi, S-N. Furukawa, M. Inoue, K. Eguchi, Autothermal reforming of methane over Ni catalysts supported over CaO-CeO₂-ZrO₂ solid solution, *Appl. Catal. A: Gen.* 240 (2003) 223-233.
24. S. Yoon, I. Kang, J. Bae, Suppression of ethylene-induced carbon deposition in diesel autothermal reforming, *Int. J. Hydrogen Energy* 34 (2009) 1844-1851.
25. C.Y. Zhao, Review on thermal transport in high porosity cellular metal foams with open cells, *Int. J. Heat Mass Tran.* 55 (2012) 3618-3632.
26. P.J. Tan, S.R. Reid, J.J. Harrigan, Z. Zou, S. Li, Dynamic compressive strength properties of aluminum foams, Part I – experimental data and observations, *J. Mech. Phys. Solids* 53 (2005) 2174-2205.
27. Y. Liang, P. Wang, H.-B. Dai, Hydrogen bubbles dynamic template preparation of a porous Fe-Co-B/Ni foam catalyst for hydrogen generation from hydrolysis of alkaline sodium borohydride solution, *J. Alloy. Compd.* 491 (2010) 359-365.
28. M.V. Twigg, J.T. Richardson, Theory and applications of ceramic foam catalysts, *Chem. Eng. Res. Des.*, 80 (2002) 183-189.
29. J.T. Richardson, Y. Peng, D. Remue, Properties of ceramic foam catalyst supports; pressure drop, *Appl. Catal. A: Gen.* 204 (2000) 19-32.
30. L. Giani, G. Groppi, E. Tronconi, Mass-transfer characterization of metallic foams as supports for structured catalysts, *Ind. Eng. Chem. Res.* 44 (2005) 4993-5002.
31. H. Tanaka, N. Mizuno, M. Misono, Catalytic activity and structural stability of La_{0.9}Ce_{0.1}Co_{1-x}Fe_xO₃ perovskite catalysts for auto motive emissions control, *Appl. Catal. A: Gen.* 244 (2003) 371-382.
32. J. Tang, M. Zhu, T. Zhong, Y. Hou, H. Wang, H. Yan, Synthesis of fine Pb(Fe_{0.5}Nb_{0.5})O₃ perovskite powders by coprecipitation method, *Mater. Chem. Phys.* 101 (2007) 475-479.
33. V.R. Choudhary, K.C. Mondal, CO₂ reforming of methane combined with steam reforming or partial oxidation of methane to syngas over NdCoO₃ perovskite-type mixed metal-oxide catalyst, *Appl. Energ.* 83 (2006) 1024-1032.

34. L. Tan, L. Yang, X. Gu, W. Jin, L. Zhang, N. Xu, Influence of the size of doping ion on phase stability and oxygen permeability of $\text{SrCO}_{0.8}\text{Fe}_{0.2}\text{O}_{3-\delta}$ oxide, *J. Membrane Sci.* 230 (2004) 21-27.
35. G.C. Araujo, S.M. Lima, J.M. Assaf, M.A. Peña, J.L.G. Fierro, M.C. Rangel, Catalytic evaluation of perovskite-type oxide $\text{LaNi}_{1-x}\text{Ru}_x\text{O}_3$ in methane dry reforming, *Catal. Today* 133-135 (2008) 129-135.
36. M.A. Peña, J.L.G. Fierro, Chemical Structures and Performance of Perovskite Oxides, *Chem. Rev.* 101 (2001) 1981-2017.
37. S. Nakamura, M. Tanaka, H. Kato, Y. Tokura, Mössbauer Study on the ordered Double Perovskite A_2FeReO_6 (A=Ca, Sr), *J. Phys. Soc. Jpn.* 72 (2003) 424-428.
38. N.K. Labhsetwar, A. Watanabe, T. Mitsuhashi, New improved synthesis of LaRu_3 perovskite and their applications in environmental catalysis, *Appl. Catal. B: Environ.* 40 (2003) 21-30.
39. J. Guo, H. Lou, Y. Zhu, X. Zheng, La-based perovskite precursors preparation and its catalytic activity for CO_2 reforming of CH_4 , *Mater. Lett.* 57 (2003) 4450-4455.
40. L. Fabbrini, I. Rossetti, L. Forni. Effect of primer on honeycomb-supported $\text{La}_{0.9}\text{Ce}_{0.1}\text{CoO}_{3+\delta}$ perovskite for methane catalytic flameless combustion, *Appl. Catal. B: Environ.* 44 (2003) 107-116.
41. C. Chettapongsaphan, S. Charojrochkul, S. Assabumrungrat, N. Laosiripojana, Catalytic H_2O and CO_2 reforming of CH_4 over perovskite-based $\text{La}_{0.8}\text{Sr}_{0.2}\text{Cr}_{0.9}\text{Ni}_{0.1}\text{O}_3$: Effects of pre-treatment and co-reactant/ CH_4 on its reforming characteristics, *Appl. Catal. A: Gen.* 386 (2010) 194-200.
42. G.R. Moradi, F. Khosravian, M. Rahmanzadeh, Effects of Partial Substitution of Ni by Cu in LaNiO_3 perovskite Catalyst for Dry Methane Reforming, *Chinese J. Catal.* 33 (2012) 797-801.
43. F. Fiévet, J.P. Lagier, B. Blin, M. Figlarz, Homogeneous and heterogeneous nucleations in the polyol process for the preparation of micron and submicron size metal particles, *Solid State Ionics* 32 (1989) 198-205.
44. J.H. Choi, D.H. Kim, J.C. Yoon, Y.J. Kim, Synthesis conditions in tailoring morphology of reticular particles in porous nickel powders prepared by

- template-assisted polyol process, *J. Alloy Compd.* 487 (2009) 8-11.
45. C.Y. Lu, H.H. Tseng, M.Y. Wey, L.Y. Liu, K.H. Chuang, Effects of the ratio of Cu/Co and metal precursors on the catalytic activity over Cu-Co/Al₂O₃ prepared using the polyol process, *Mat. Sci. Eng. B* 157 (2009) 105-112.
 46. X. Zhai, Y. Cheng, Z. Zhang, Y. Jin, Y. Cheng, Steam reforming of methane over Ni catalyst in micro-channel reactor, *Int. J. Hydrogen Energy* 36 (2011) 7105-7113.
 47. J.T. Richardson, D. Remue, J.-K. Hung, Properties of ceramic foam catalyst supports: mass and heat transfer, *Appl. Catal. A: Gen.* 250 (2003) 319-329.
 48. Y. Demirel, R.N. Sharma, H.H. Al-Ali, On the effective heat transfer parameters in a packed bed, *Int. J. Heat Mass Tran.* 43 (2000) 327-332.
 49. D.E. Beasley, J.A. Clark, Transient response of a packed bed for thermal energy storage, *Int. J. Heat Mass Tran.* 27 (1984) 1659-1669.
 50. K. Boomsma, D. Poulikakos, F. Zwick, Metal foams as compact high performance heat exchangers, *Mech. Mater.* 35 (2003) 1161-1176.
 51. K.Y. Koo, H.-S. Roh, Y.T. Seo, D.J. Seo, W.L. Yoon, S.B. Park, A highly effective and stable nano-sized Ni/MgO-Al₂O₃ catalyst for gas to liquids (GTL) process, *Int. J. Hydrogen Energy* 33 (2008) 2036-2043.
 52. W.J. Lee, C.-Z. Li, Coke formation and reaction pathways of catalyst-surface-generated radicals during the pyrolysis of ethane using Ni mesh catalyst, *Appl. Catal. A: Gen.* 316 (2007) 90-99.
 53. N. Wang, X. Yu, Y. Wang, W. Chu, M. Liu, A comparison study on methane dry reforming with carbon dioxide over LaNiO₃ perovskite catalysts supported on mesoporous SBA-15, MCM-41 and silica carrier, *Catal. Today* 212 (2013) 98-107.
 54. W. Wu, W. Guan, G. Wang, W. Liu, Q. Zhang, T. Chen, W.G. Wang, Evaluation of Ni₈₀Cr₂₀/(La_{0.75}Sr_{0.25})_{0.95}MnO₃ dual layer coating on SUS430 stainless steel used as metallic interconnect for solid oxide fuel cells, *Int. J. Hydrogen Energy* 39 (2014) 996-1004.
 55. G.S. Gallego, F. Mondragón, J.M. Tatibouët, J. Barrault, C. Batiot-Dupeyrat, Carbon dioxide reforming of methane over La₂NiO₄ as catalyst precursor-

- Characterization of carbon deposition, Catal. Today 133-135 (2008) 200-209.
56. G.S. Gallego, C. Batiot-Dupeyrat, J. Barrault, E. Florez, F. Mondragón, Dry reforming of methane over $\text{LaNi}_1\text{-BO}_{3\pm\delta}$ (B=Mg, Co) perovskites used as catalyst precursor, Appl. Catal. A: Gen. 334 (2008) 251-258.

Curriculum Vitae

Name: 박 대 일 (朴 大 逸, Daeil Park)

Date of Birth: Jan 04. 1985

E-mail: kazami1211@gmail.com

Nationality: Republic of Korea

Education

03/2012 - 08/2015 : Ph.D., Daeil Park, Department of Aerospace engineering, Chosun
University, Gwang-ju, Republic of Korea

03/2010 - 02/2012 : M.S., Daeil Park, Department of Aerospace engineering, Chosun
University, Gwang-ju, Republic of Korea

03/2003 - 02/2010 : B.S., Daeil Park, Department of Aerospace engineering, Chosun
University, Gwang-ju, Republic of Korea

Society Membership

KSME (Korea Society of Mechanical Engineers), Student member

KSAS (Korean Society for Aeronautical and Space Science), Student member

KICHe (The Korean Institute of Chemical Engineers), Student member

KSPE (Korean Society for Propulsion Engineers), Student member

KHNES (The Korean Hydrogen & New Energy Society), Student member

Award

- [1] Daeil Park, " Study of Co-Ni-P-B/Ni foam catalysts for hydrogen generation from alkaline NaBH_4 solution", The Korean Hydrogen & New Energy Society, Best Oral presentation, 2010.

Patent

- [1] Daeil Park, Dong Ju Moon, Taegyu Kim, "A high-durability metal foam supported catalyst for compositive reforming steam-carbon dioxide and manufacture method thereof", 10-2012-0132551, Republic of Korea.
- [2] Daeil Park, Dong Ju Moon, Taegyu Kim, "Metal Foam-supported Catalyst for Steam Carbon Dioxide Reforming and Method For Preparing the Same", 13/909,412., United State.
- [3] Daeil Park, Dong Ju Moon, Taegyu Kim, "Manufacturing method of perovskite-type nuckel based catalyst", 10-2014-0060540, Republic of Korea.

International Journals

- [1] Daeil Park, Dong Ju Moon, Taegyu Kim, "Steam- CO_2 refoming of methane on $\text{Ni}/\gamma\text{-Al}_2\text{O}_3$ -deposited metallic foam catalyst for GTL-FPSO process", *Fuel Processing Technology*, 2013, 112, 28-34.
- [2] Daeil Park, Dong Ju Moon, Taegyu Kim, "Preparation and Evaluation of a Metallic Foam Catalyst for Steam- CO_2 Reforming of Methane in GTL-FPSO

- Process", *Fuel Processing Technology*, 2014, 124, 97-103.
- [3] Daeil Park, Jong Wook Bae, Dong Ju Moon, Taegyu Kim, "Modified nano-particulate perovskite catalyst for steam and CO₂ reforming of methane", *Journal of Nanoscience and Nanotechnology*, 2015, 15, 5889-5892.
- [4] Daeil Park, Dong Ju Moon, Taegyu Kim, "Effect of polyvinyl-pyrrolidone in a polyol method on preparation of perovskite-type catalyst for steam-CO₂ reforming of methane", *International Journal of Hydrogen Energy*, 2015, 40, 1481-1489.
- [5] Daeil Park, ChangWook Lee, Dong Ju Moon, Taegyu Kim, "Novel macro-micro channel reactor for reforming glycerol produced from biodiesel productions", *Energy Procedia*, In press.
- [6] Daeil Park, Taegyu Kim, "Electroless Plated Co-Ni-P-B/Ni foam catalyst for hydrogen generation from sodium borohydride", *Journal of Nanoscience and Nanotechnology*, In press.
- [7] Daeil Park, Dong Ju Moon, Taegyu Kim, "Design, analysis, and performance evaluation of steam-CO₂ reforming reactor for syngas production in GTL process", *International Journal of Hydrogen Energy*, In press.

International Conferences

- [1] 06/2012, Daeil Park, Taegyu Kim, "Design, analysis, and performance evaluation of SCR reactor for syngas production in GTL process", *International conference on hydrogen production-2012*, Seoul, Republic of Korea.
- [2] 03/2013, Daeil Park, Dong Ju Moon, Taegyu Kim, "Preparation, Characterization

- and Performance Evaluation of Metallic Foam Catalyst for Steam-CO₂ reforming of Methane" *10th Natural Gas Conversion Symposium*, Doha, Qatar.
- [3] 08/2013, Daeil Park, Dong Ju Moon, Taegyu Kim, "Heat transfer improvement of metallic foam catalyst for Steam-CO₂ reforming reaction", ANBRE13, Seoul, Republic of Korea.
- [4] 08/2013, Daeil Park, Dong Ju Moon, Taegyu Kim, "Structured perovskite type catalyst for Steam-CO₂ reforming of methane", WCCE9 & APCChE, Seoul, Republic of Korea.
- [5] 11/2013, Daeil Park, Dong Ju Moon, Taegyu Kim, "Modified nano-perovskite catalysts for the steam and CO₂ reforming of methane", ICNST2013, Gwang-ju, Republic of Korea.
- [6] 05/2014, Daeil Park, ChangWook, Lee, Dong Ju Moon, Taegyu Kim, "Novel macro-micro channel reactor for refoming glycerol produced from biodiesel productions" ICAE2014, Taipei, Taiwan.
- [7] 09/2014, Daeil Park, Dong Ju Moon, Taegyu Kim, "Effect of PVP in polyol method on the perovskite-type catalyst for carbon dioxide reforming of methane", WHEC2014, Gwang-ju, Republic of Korea.
- [8] 09/2014, Daeil Park, Dong Ju Moon, Taegyu Kim, "effect of gelation agents on La_{1-x}Sr_xNiO₃ perovskite-type catalyst for steam-CO₂ reforming of methane", ISCRE 23 & APCRE 7, Bangkok, Thailand.
- [9] 11/2014, Daeil Park, Taegyu Kim, "Electroless Plated Co-Ni-P-B/Ni foam catalyst for hydrogen generation from sodium borohydride", ICNST 2014, Mokpo,

Republic of Korea.

- [10] 11/2014, Daeil Park, ChangWook Lee, Dong Ju Moon, Taegyu Kim, "Preparation and evaluation of a supported catalyst for glycerol steam reforming", ICNST 2014, Mokpo, Republic of Korea.

Domestic Conferences

- [1] 11/2011, Daeil Park, Taegyu Kim, "Design and thermal-fluidic analysis of SCR reactor for GTL-FPSO", Proceedings of KSME Annual Fall Meeting, Daegu, Republic of Korea.
- [2] 11/2011, Daeil Park, Taegyu Kim, "Performance evaluation of natural gas SCR reactor for clean aviation fuel production", Proceedings of KSAS Annual Fall Meeting, Pyeongchang, Republic of Korea.
- [3] 04/2012, Daeil Park, Taegyu Kim, "Performance evaluation of Ni-based metal foam catalyst for SCR reaction", Proceedings of KICChE Annual Spring Meeting, Jeju, Republic of Korea.
- [4] 05/2012, Daeil Park, Taegyu Kim, "Study of metal foam catalyst for CH₄ SCR reaction for GTL-FPSO process", Proceedings of KHNES Annual Spring Meeting, Seoul, Republic of Korea.
- [5] 05/2012, Daeil Park, Taegyu Kim, "Study of reforming catalyst for synthesis gas for GTL-FPSO process" Proceedings of KSPE Annual Spring Meeting, Gumi, Republic of Korea.
- [6] 10/2012, Daeil Park, Dong Ju Moon, Taegyu Kim, "Performance comparison of

- metallic foam catalyst to pelletized catalyst for SCR reaction", Proceedings of KIChE Annual Fall Meeting, Busan, Republic of Korea.
- [7] 04/2013, Daeil Park, Dong Ju Moon, Taegyu Kim, "Thermal-fluidic analysis of MM channel reactor for reforming of glycerol", Proceedings of KIChE Annual Spring Meeting, Gwang-ju, Republic of Korea.
- [8] 04/2013, Daeil Park, Dong Ju Moon, Taegyu Kim, "Performance comparison of perovskite type metal foam and powder catalyst for SCR reaction", Proceedings of KIChE Annual Spring Meeting, Gwang-ju, Republic of Korea.